JPEDAV (2009) 30:517–534
DOI: 10.1007/s11669-009-9570-6
1547-7037 ©ASM International

First-Principles Calculations and CALPHAD Modeling of Thermodynamics

Zi-Kui Liu

(Submitted April 11, 2009)

Thermodynamics is the key component of materials science and engineering. The manifestation of thermodynamics is typically represented by phase diagrams, traditionally for binary and ternary systems. Consequently, the applications of thermodynamics have been rather limited in multicomponent engineering materials. Computational thermodynamics, based on the CALPHAD approach developed in the last few decades, has released the power of thermodynamics and enabled scientists and engineers to make phase stability calculations routinely for technologically important engineering materials. Within the similar time frame, first-principles quantum mechanics technique based on density functional theory has progressed significantly and demonstrated in many cases the accuracy of predicted thermodynamic properties comparable with experimental uncertainties. In this paper, the basics of the CALPHAD modeling and first-principles calculations are presented emphasizing current multiscale and multicomponent capability. Our research results on integrating first-principles calculations and the CALPHAD modeling are discussed with examples on enthalpy of formation at 0 K, thermodynamics at finite temperatures, enthalpy of mixing in binary and ternary substitutional solutions, defect structure and lattice preference, and structure of liquid, super-cooled liquid, and glass.

Keywords ab initio methods, CALPHAD, CALPHAD approach, computational studies, first principles, thermodynamics

1. Introduction

The development of new materials and the capability to tailor existing materials to meet new and demanding applications are critical for continued improvements in the quality of human life. Traditionally, the field of materials science and engineering has predominately focused on processing materials, establishing structure-property relations, and measuring material properties. This empirical approach is increasingly shifting toward the design of materials to achieve optimal functionality, driven by advances in computational materials science and information technology, particularly in the last few decades. Today, we are witnessing a paradigm shift in materials research and development from experimental based knowledge creation to integrated computational-prediction and experimental-validation approaches.[1-4]

The computational prediction of materials performance requires reliable thermodynamic and kinetic data. For over 30 years, a thermodynamic modeling technique, widely known as the calculation of phase diagrams (CALPHAD) method, has shown to be a viable approach in developing thermodynamic databases and calculating phase equilibria in multicomponent materials.[5,6] The CALPHAD method was pioneered by Kaufman,[7-10] who systematically introduced the foundational concept of lattice stability, i.e., the Gibbs energy difference between the stable structure and other structures of pure element, the methodology to evaluate them in the multidimensional space of temperature, pressure, and compositions, and their integration into multicomponent systems, which was later extended to model multicomponent atomic mobility[11,12] and molar volume.[13,14] It seems certain that the CALPHAD method will be extended further to model a wide range of materials properties as a function of temperature, pressure, and compositions because this method provides a hierarchical mechanism to build multicomponent property databases starting from pure elements to binary and ternary systems.

Modeling is a bridge between experimental observations and theoretical predictions, as is the CALPHAD modeling. From the beginning of the development of CALPHAD, fundamental physical and chemical approaches in phase stability were part of the discussions.[8,15,16] This was also reflected in publications in the first volume of the CALPHAD journal,[17-20] including approaches to predictions of materials properties such as the tight binding model,

This article is an invited paper selected from participants of the 14th National Conference and Multilateral Symposium on Phase Diagrams and Materials Design in honor of Prof. Zhanpeng Jin's 70th birthday, held November 3-5, 2008, in Changsha, China. The conference was organized by the Phase Diagrams Committee of the Chinese Physical Society with Drs. Huashan Liu and Libin Liu as the key organizers. Publication in *Journal of Phase Equilibria and Diffusion* was organized by J.-C. Zhao, The Ohio State University; Yong Du, Central South University; and Qing Chen, Thermo-Calc Software AB.

Zi-Kui Liu, Department of Materials Science and Engineering, The Pennsylvania State University, University Park, PA 16802. Contact e-mail: dr.liu@psu.edu.

ab initio pseudopotentials, distorted Wigner-Seitz cells, and pair potentials. Over the last 50 years, both theoretical predictions and CALPAHD modeling have progressed significantly and interacted intensively, as evidenced the development of CALPHAD lattice stability,[21,22] the series of Ringberg workshops on integration of first-principles calculations and CALPAHD modeling,[23-25] and systematic first-principles calculations of lattice stability[26,27] and energy of formation[28] along with advanced tools for the CALPHAD modeling[29] and first-principles calculations.[25] Many issues have been resolved to bring them closer, particularly the energy of formation of stable compounds,[28] but serious discrepancies still exist for the lattice stability of some elements.[30] There have been considerable efforts in recent years to address the lattice stability issue for pure elements.[27,31-34] The ab initio molecular dynamics (AIMD) approach employed recently by Ozolins for fcc and bcc W[34]seems to be particularly promising. The AIMD approach will be discussed in more detail in a later section of this paper. For nonstoichiometric compounds with more than one type of Wyckoff positions, lattice stability from first-principles calculations has been used without detailed discussions on the instability issue.[35-39]

This paper aims to give an overview on the CALPHAD modeling and first-principles calculations based on our research activities in the past several years. It is organized as following. In Section 2, the CALPHAD modeling of thermodynamics is presented. The fundamentals and approximations of first-principles calculations are discussed in Section 3 in terms of total energy at 0 K, multiscale entropic contributions including mixing of atoms, lattice vibration, thermal electrons and spin polarization, and AIMD calculations. In Section 4, our research results in integrating first-principles calculations and the CALPHAD modeling are summarized in six areas, i.e., enthalpy of formation at 0 K, thermodynamics at finite temperatures, magnetic property and magnetic transition, enthalpy of mixing in binary and ternary substitutional solutions, defect structure and lattice preference, and structure of liquid, super-cooled liquid, and glass. The last parts of the paper are summary, acknowledgements, and references.

2. CALPHAD Modeling of Thermodynamics

Since the pioneering work by Kaufman who also coined the name CALPHAD,[10] the CALPHAD modeling of thermodynamics has been developed into a sophisticated approach capable of calculating phase equilibria in multicomponent, technologically important materials. The history of CALPHAD was recently reviewed briefly by Spencer,[6] and several books have been devoted completely or extensively to this topic.[40-42] The CALPHAD approach is based on mathematically formulated models describing the thermodynamic properties of individual phases. The model parameters are evaluated from thermochemical data of individual phases and phase equilibrium data between phases as shown schematically in Fig. 1. The CALPHAD

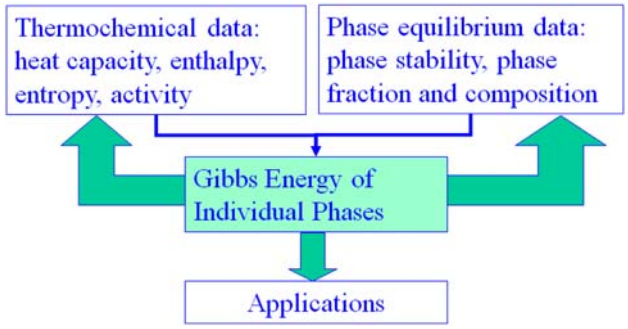

Fig. 1 Schematic diagram showing the contributions of thermochemical and phase equilibrium data to the CALPHAD modeling

approach is particularly valuable in materials science and engineering in comparison with physics and chemistry due to more complicated systems involving multicomponent solution phases.

In practical applications of materials, the commonly controlled processing variables are temperature (T), pressure (P), and number of atoms or moles of component i (N_i), which render the Gibbs energy (G) to be the state function to be modeled as T, P, and N_i are its natural variables and used in the CALPHAD modeling. While most theoretical considerations are related to the interactions between atoms, the atomic distance or volume (V) thus becomes a controlling/independent variable as in typical first-principles calculations, and the Helmholtz energy (F) with T, V, and N_i as its natural variables becomes the state function to be modeled. These two state functions are exchangeable through the following equations

$$G(T,P,N_i) = F + PV = F - \frac{\partial F}{\partial V}V \qquad \text{(Eq 1)}$$

$$F(T,V,N_i) = G - PV = G - P\frac{\partial G}{\partial P} \qquad \text{(Eq 2)}$$

In the CALPHAD modeling, the molar Gibbs energy of individual phases is modeled. With most solid phases having more than one sublattice, i.e., nonequivalent Wyckoff sites, the compound energy formalism[43] has been developed to take the existence of the sublattices into account. In a recent review, Hillert[44] presented the progress of the compound energy formalism, its applications to various complex problems, and recent developments including treatments of short range order. Short range order has been typically treated with the pair approximation quasichemical model[45-47] and more recently by the cluster site approximation.[48] The discussion of this paper focuses on the compound energy formalism.

Let us use $(A_i\cdots)_a(B_j\cdots)_b(C_k\cdots)_c\cdots$ to represent a solution phase, α, with multicomponents and multisublattices. Each set of parentheses denotes one sublattice with the letters inside the parentheses designating the elements in the sublattice and the subscript outside the parentheses the number of the sublattice site. The molar Gibbs energy of the

α phase can be written in general as follows in terms of per mole of formula (mf)

$$G^{\alpha}_{\mathrm{mf}} = \sum_{A_i,B_j,C_k\cdots}\left(\prod_p y^p_q\right)G^{\Phi}_{A_i:B_j:C_k\cdots} + \Delta G^{\alpha/\Phi}_{\mathrm{mf}} \qquad \text{(Eq 3)}$$

In the above equation, the summation goes over all the elements in each sublattice and the product of site fractions, y^p_q, goes over all sublattices, p, with one element, q, in the corresponding sublattice, representing the reference Gibbs energy of the α phase. $G^{\Phi}_{A_i:B_j:C_k\cdots}$ is the Gibbs energy of a structure Φ with one element in each sublattice, $(A_i)_a(B_j)_b(C_k)_c\ldots$, called end-members or compounds, and $\Delta G^{\alpha/\Phi}_{\mathrm{mf}}$ is the Gibbs energy difference between the α phase and the reference Gibbs energy. The semicolon separates sublattices. When all the end-members are chosen to have the same structure as the α phase, $\Delta G^{\alpha/\Phi}_{\mathrm{mf}}$ denotes the Gibbs energy of mixing $\Delta G^{\mathrm{mix}}_{\mathrm{mf}}$. When the end-members have their respective, often stable, structures different from that of the α phase, $\Delta G^{\alpha/\Phi}$ is referred as the Gibbs energy of formation $\Delta_f G_{\mathrm{mf}}$ with respect to the chosen structures of the end-members.

It is in the modeling of the Gibbs energy of mixing that the concept of lattice stability is needed. In the case that the α phase has only one sublattice, i.e., a substitutional solution, $G^{\alpha}_{A_i}$ represents the Gibbs energy of pure A_i in the structure α, even though α may not be the stable structure of pure A_i. Consequently, the Gibbs energy difference between the stable structure (SER, stable element reference) and the structure α is needed in order to describe the whole composition range of the α phase. This Gibbs energy difference is referred to as the lattice stability of A_i in the structure α and defined as

$$\Delta G^{\alpha}_{A_i} = G^{\alpha}_{A_i} - G^{\mathrm{SER}}_{A_i} \qquad \text{(Eq 4)}$$

Similarly, when the α phase has more than one sublattice, the lattice stability of the end-member can be defined as the following

$$\Delta G^{\alpha}_{A_i:B_j:C_k\cdots} = G^{\alpha}_{A_i:B_j:C_k\cdots} - \sum z G^{\mathrm{SER}}_x \qquad \text{(Eq 5)}$$

where x is one of the elements and z the number of sublattice sites which x is in, and the summation goes over all elements in the end-member. In the framework of SGTE (Scientific Group of Thermodata Europe), Dinsdale[49] compiled the Gibbs energy functions of pure elements derived from the heat capacity and enthalpy of transition, and their common lattice stability from various extrapolations. The Gibbs energy functions take the following general form as a function of temperature in per mole of atoms

$$G_{\mathrm{m}} = a + bT + cT\ln(T) + \sum d_n T^n \qquad \text{(Eq 6)}$$

These Gibbs energy functions are widely used in the CALPHAD modeling. It should be pointed out that a common lattice stability framework for end-members remains to be developed due to the lack of data, and the first-principles calculations have the potential to contribute significantly.[36-38]

In modeling the Gibbs energy of mixing, one usually separates it into ideal $\left(\Delta^{\mathrm{id}}G^{\mathrm{mix}}_{\mathrm{mf}}\right)$ and nonideal $\left(\Delta^{\text{non-id}}G^{\mathrm{mix}}_{\mathrm{mf}}\right)$ mixing components with the latter sometimes called excess Gibbs energy of mixing $\Delta^{\mathrm{xs}}G^{\mathrm{mix}}_{\mathrm{mf}}$. The ideal mixing assumes mechanical mixing among atoms in each sublattice without interactions between atoms, i.e., all atomic bonds are identical. There is thus only an entropic contribution from the random distribution of atoms in each sublattice, i.e.,

$$\Delta^{\mathrm{id}}G^{\mathrm{mix}}_{\mathrm{mf}} = RT\sum z\sum y_i \ln y_i \qquad \text{(Eq 7)}$$

where the first summation goes over all sublattices and the second summation goes over all elements in that sublattice. In real materials, the atomic bonding characteristics between different atoms are unique, and the atomic mixing would thus result in additional Gibbs energy change with preferred local atomic arrangements, i.e., short-range ordering. This can cause miscibility gaps, order-disorder transitions, or the formation of compounds depending on the sign and magnitude of the excess Gibbs energy of mixing $(\Delta^{\mathrm{xs}}G^{\mathrm{mix}}_{\mathrm{mf}})$. The widely used mathematical formula for $\Delta^{\mathrm{xs}}G^{\mathrm{mix}}_{\mathrm{mf}}$ is the Redlich-Kister polynomial[50] shown below:

$$\begin{aligned}
&\Delta^{\mathrm{xs}}G^{\mathrm{mix}}_{\mathrm{mf}}\\
&= \sum y^{\mathrm{II}}_{B_j}y^{\mathrm{III}}_{C_k}\cdots\sum y^{\mathrm{I}}_{A_{i1}}y^{\mathrm{I}}_{A_{i2}}\sum_m {}^mL_{A_{i1},A_{i2}:B_j:C_k\cdots}\left(y^{\mathrm{I}}_{A_{i1}}-y^{\mathrm{I}}_{A_{i2}}\right)^m\\
&+\sum y^{\mathrm{I}}_{A_i}y^{\mathrm{III}}_{C_k}\cdots\sum y^{\mathrm{II}}_{B_{j1}}y^{\mathrm{II}}_{B_{j2}}\sum_m {}^mL_{A_i:B_{j1},B_{j2}:C_k\cdots}\left(y^{\mathrm{II}}_{B_{j1}}-y^{\mathrm{II}}_{B_{j2}}\right)^m\\
&+\sum y^{\mathrm{I}}_{A_i}y^{\mathrm{II}}_{B_j}\cdots\sum y^{\mathrm{III}}_{C_{k1}}y^{\mathrm{III}}_{C_{k2}}\sum_m {}^mL_{A_i:B_j,C_{k1},C_{k2}\cdots}\left(y^{\mathrm{III}}_{C_{k1}}-y^{\mathrm{III}}_{C_{k2}}\right)^m\\
&+\cdots+\sum y^{\mathrm{III}}_{C_k}\cdots\sum y^{\mathrm{I}}_{A_{i1}}y^{\mathrm{I}}_{A_{i2}}y^{\mathrm{II}}_{B_{j1}}y^{\mathrm{II}}_{B_{j2}}L^{\mathrm{SRO}}_{A_{i1},A_{i2}:B_{j1},B_{j2}:C_k\cdots}\\
&+\sum y^{\mathrm{II}}_{B_j}\cdots\sum y^{\mathrm{I}}_{A_{i1}}y^{\mathrm{I}}_{A_{i2}}y^{\mathrm{III}}_{C_{k1}}y^{\mathrm{III}}_{C_{k2}}L^{\mathrm{SRO}}_{A_{i1},A_{i2}:B_j:C_{k1},C_{k2}\cdots}\\
&+\sum y^{\mathrm{I}}_{A_j}\cdots\sum y^{\mathrm{II}}_{B_{j1}}y^{\mathrm{II}}_{B_{j2}}y^{\mathrm{III}}_{C_{k1}}y^{\mathrm{III}}_{C_{k2}}L^{\mathrm{SRO}}_{A_i:B_{j1}:B_{j2}:C_{k1},C_{k2}\cdots}+\cdots\\
&+\sum y^{\mathrm{II}}_{B_j}y^{\mathrm{III}}_{C_k}\cdots\sum y^{\mathrm{I}}_{A_{i1}}y^{\mathrm{I}}_{A_{i2}}y^{\mathrm{I}}_{A_{i3}}\left(y^{\mathrm{I}}_{A_{i1}}I^{\mathrm{I}}_{A_{i1}}+y^{\mathrm{I}}_{A_{i2}}I^{\mathrm{I}}_{A_{i2}}+y^{\mathrm{I}}_{A_{i3}}I^{\mathrm{I}}_{A_{i3}}\right)
\end{aligned} \qquad \text{(Eq 8)}$$

where ${}^mL$ is the mth binary interaction parameters with colons separating elements between sublattices and comma separating interacting elements in the same sublattice, L^{SRO} is the reciprocal interaction parameter to approximate the effect of short range ordering (SRO),[51,52] and I^I are the ternary interaction parameters. As an example, the composition square for a reciprocal solution defined as $(A,B)_a(C,D)_b$ is shown in Fig. 2(a) with its site fractions and interaction parameters indicated. The Gibbs energy of end-members and the Gibbs energy surface of end-members, i.e., the summation in Eq 3, are depicted in Fig. 2(b). The ideal entropy of mixing represented by Eq 7 makes the Gibbs energy concave, and further adjustment of the Gibbs energy surface is realized by the interaction parameters. This reciprocal solution is used to represent an ordering solution when A and C are identical and B and D are identical such as the $L1_2$ phase in the Fe-Ni system shown in Fig. 3.[53]

In the common practice of the CALPHAD modeling, the interaction parameters usually take the form of $A + BT$ with

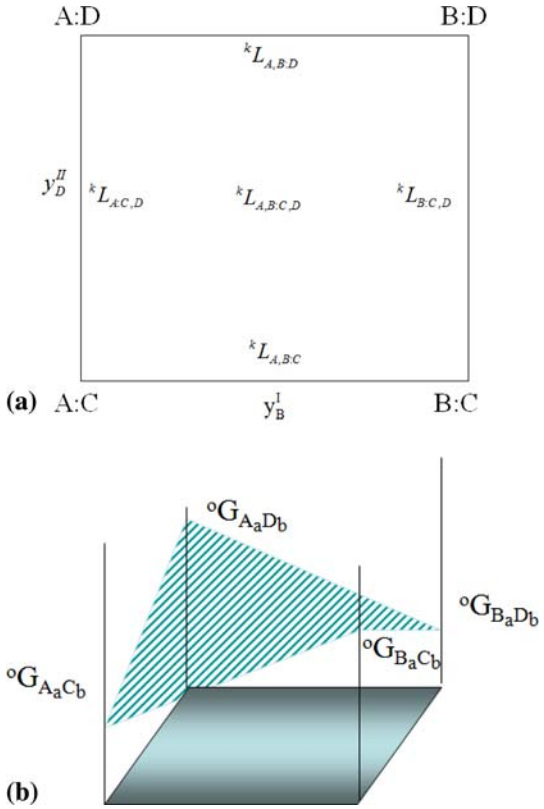

Fig. 2 Composition square and interaction parameters for a reciprocal solution, $(A,B)_a(C,D)_b$, (a), and corresponding Gibbs energy surface of end-members (b)

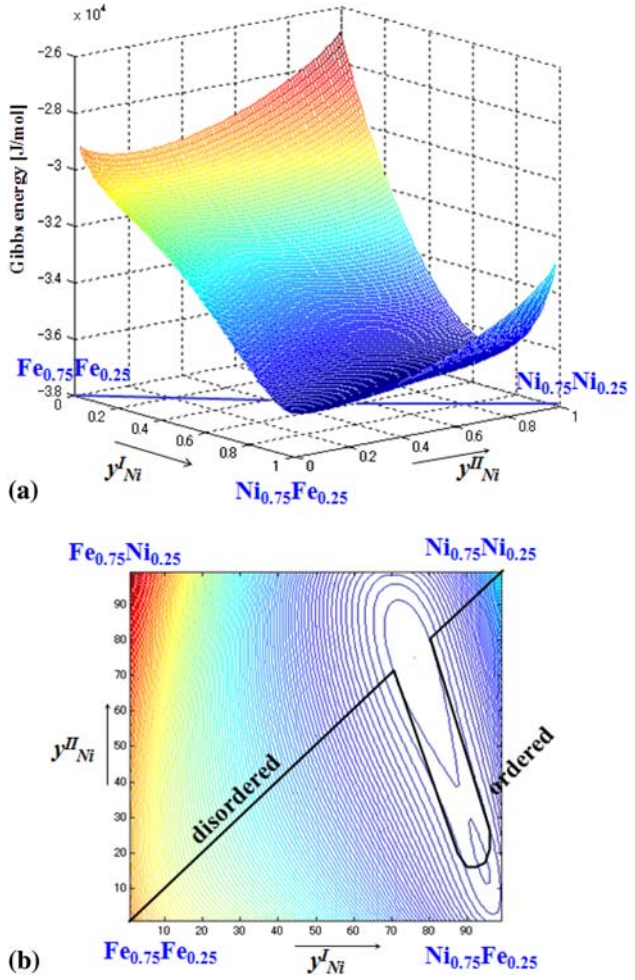

Fig. 3 Three-dimensional plot of the Gibbs energy of $L1_2$ $(Fe,Ni)_{0.75}(Fe,Ni)_{0.25}$ at 530 °C (a) and its projection to the composition square (b), noting the miscibility gap between the ordered and disordered phases[53]

A and *B* being the model parameters, and the order of interaction parameters, *m*, is between 0 and 2. These interaction model parameters and the lattice stability of end-members (see Eq 4 and 5) are evaluated from thermochemical data that is directly related to derivatives of the Gibbs energy of individual phases and phase equilibrium data where the chemical potential of an element has the same value in all phases in equilibrium. The thermochemical and phase equilibrium data were primarily from experimental investigations until quite recently that first-principles calculations are able to provide quantitatively accurate data (see references cited in Section 1). It should be emphasized that phase equilibrium data not only demands very high accuracy on the relative values of the Gibbs energy of phases, usually in the range of Joules or tens of Joules, but also makes model parameters in a database closely related to each other. This close relationship among model parameters means that if one model parameter in one phase is modified, all other model parameters, whether directly or indirectly related to the modified parameter through phase equilibria, need to be re-evaluated. Furthermore, from Eq 3 and the equations that follow, it is self-evident that the Gibbs energy of a phase depends on both lattice stability and interaction parameters. It is important that both parameters are physically sound, as pointed out by Kaufman early in the development of this approach.[8]

The sublattice models in the compound energy formalism are derived from crystal structures of phases. The simplest approach is to define all Wyckoff sites as separate sublattices.[54] However, this often introduces many end-members for complex phases, and there is often not enough data to evaluate all the model parameters for both the end-members and the interaction parameters. Consequently, some similar sublattices are combined by taking into account elemental site occupation preferences, coordination numbers, and point symmetries.[54] Care must be taken when combining sublattices as the model parameters may become dependent on each other.[2,55]

The magnetic contribution to the Gibbs energy is considered for magnetic elements such as Fe, Co, and Ni by the following expression[56]

$$\Delta G^{\text{mag}} = RTf(T/T_C)\ln(\beta+1) \qquad \text{(Eq 9)}$$

with T_C being the magnetic transition temperature, $f(T/T_C)$ an empirical polynomial with different expressions above and below the magnetic transition temperature to reproduce the corresponding heat capacity,[56] and β the Bohr magnetic

moment. The composition dependency of T_C and β are modeled using equations similar to those in the Gibbs energy model shown above.

3. First-Principles Calculations

First-principles calculations, based on density functional theory,[57] require only knowledge of the atomic species and crystal structure and yield quantities related to the electronic structure and total energy of a given structure. For thermodynamic properties of alloys, one currently needs to calculate three additive contributions to the free energy

- The static energy or the 0 K total energy. In this case, the atoms are kept fixed at their static lattice positions.
- For thermodynamic properties at finite temperatures, the contribution of lattice thermal vibration needs to be taken into account based on the lattice dynamics or phonon approach. This also contributes to the so-called zero-point energy.
- When the electronic density of states (DOSs) at the Fermi level is high, the thermal electronic contribution needs to be included.

Therefore, in a system with an atomic volume V at temperature T, the Helmholtz energy $F(V, T)$ is the summation of the above three contributions written as[58]

$$F(V,T) = E_c(V) + F_{ph}(V,T) + F_{el}(V,T) \qquad \text{(Eq 10)}$$

For magnetic structures, spin polarizations can be added to the above calculations and contribute to each energy term in Eq 10. In this section, the fundamentals and approximations in first-principles calculations based on density functional theory are briefly presented, and the methodologies in calculating the above contributions to the Helmholtz energy are discussed. For example, the 0 K total energy, phonon dispersion curves from which phonon density of states (DOSs) can be obtained, and electronic DOS of ferromagnetic fcc Ni are shown in Fig. 4.[59]

3.1 First-Principles Calculations of Total Energy at 0 K

A solid can be thought of as a collection of interacting, positively charged nuclei and negatively charged electrons and can theoretically be treated by solving the many-body Schrödinger equation involving both the nuclei and the electrons. However, it is extremely difficult to solve the equation due to its many-body nature. Several levels of approximations have been introduced to obtain numerical solutions to the Schrödinger equation.

The first approximation is the adiabatic or Born-Oppenheimer approximation.[60] Since the nuclei are much heavier than the electrons, it can be assumed that the electrons are always in an instantaneous ground state with the nuclei. The positions of the nuclei can thus be fixed by solving the many-body Schrödinger equation for the electrons only. Since the nuclei are "frozen," they only contribute to an external potential for the electrons.

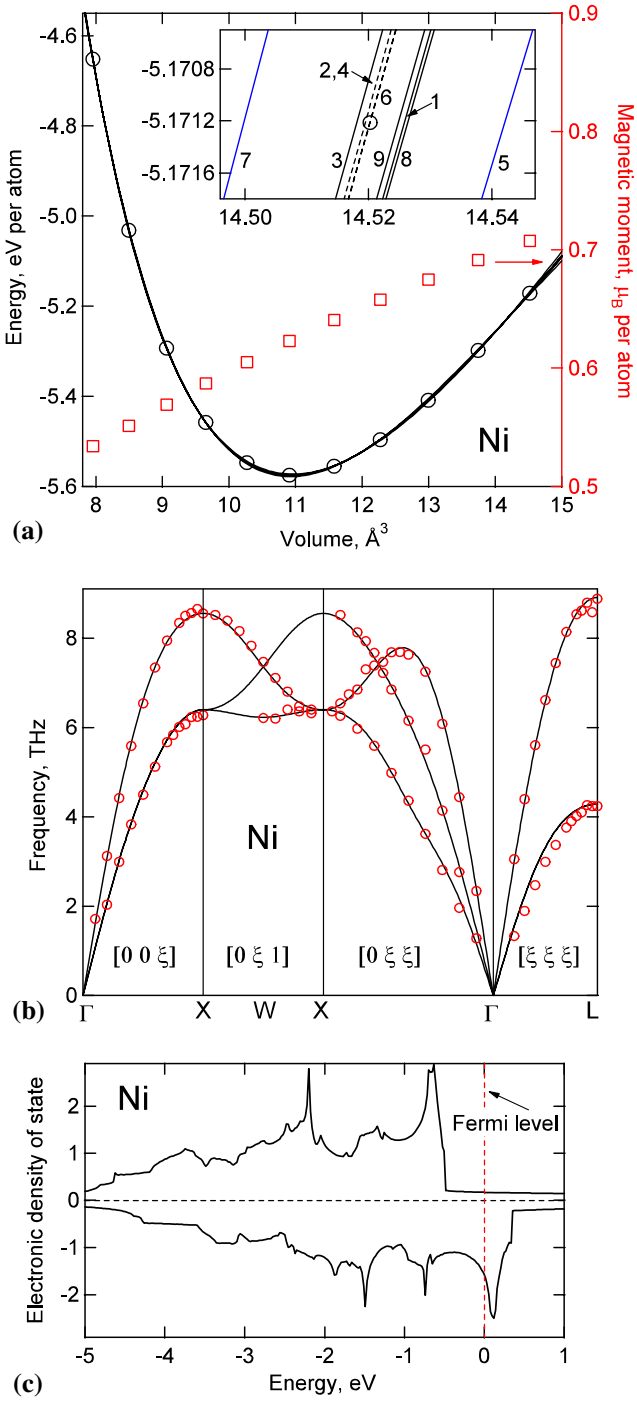

Fig. 4 0 K total energy (*open cycles*) and magnetic moment (*open squares*) with numbers for various fitted EOS (a), measured (*open cycles*) and calculated (*lines*) phonon dispersion curves (b), and electronic DOSs (c), of ferromagnetic fcc Ni[59]

The second approximation is the independent-electron approximation. Each electron moves independently of the others in an average effective potential collectively determined by all of the electrons. The key challenge has been to use this approximation to effectively describe the many-body electron-electron interactions. The early Hartree-Fock

approximation neglects all correlations except those required by the Pauli exclusion principle. The modern density functional theory (DFT) by Hohenberg and Kohn[61] is formulated as an exact theory of many-body systems. It states that a universal functional for the energy can be defined in terms of the electron density, and the potential of a system of interacting electrons is determined uniquely by the ground state electron density. The Kohn-Sham approach replaces the many-body electron problem using independent electrons with an exchange-correlation functional of the electron density and an associated exchange-correlation energy and potential.[57] By explicitly separating the independent-electron kinetic energy and long-range Coulomb interaction energy, the exchange-correlation energy can be approximated as a local functional of the electron density.

The third approximation is the exchange-correlation functional approximation that describes the exchange-correlation energy. In the local spin density approximation (LSDA),[62] the exchange-correlation energy density at each point in space is assumed to be the same as in a homogenous electron gas with the same electron density. Exchange and correlation energies for a homogenous electron gas are available based on the Ceperley-Alder[62] and Perdew-Zunger[63] fittings. The rationale for this approximation is that in many solids, the range of exchange and correlation is relative short. On the other hand, the generalized gradient approximation (GGA)[64,65] stipulates that the exchange-correlation energy density depends additionally on the gradient of the electron density. The GGA is accomplished by a low-order expansion of the exchange-correlation energy of an electron gas. Numerous approaches have been developed for this low-order expansion including the widely used PW91[66] and PBE[67] implementations. Most approaches give similar results for small electron density gradients, but appreciably different values for large gradients.

The fourth is the replacement of the strong Coulomb potential of the nucleus and the tightly bound core electrons by a pseudopotential, an effective potential acting on valence electrons. Pseudopotentials obtained from atomic calculations are not unique and can be tailored to simplify calculations such as the commonly used ultrasoft pseudopotentials and the projector augmented wave (PAW) method.[68] The PAW method keeps the full all-electron wavefunction, while in the pseudopotential approach a smooth pseudofunction is used which is required to match only the value of the all-electron wavefunction at a given radius and is more computationally efficient.

With above approximations, the DFT-based first-principles calculations solve a set of one-electron Schrödinger's equations, one for each electron in the system:

$$\left[-\frac{\hbar^2}{2m_e}\nabla^2 - \frac{e^2}{4\pi\varepsilon_0}\sum_{I=1}^{N}\frac{Z_I}{|\vec{r}-\vec{R}_I|} + \frac{e^2}{4\pi\varepsilon_0}\int\frac{\rho(\vec{r}\,')}{|\vec{r}-\vec{r}\,'|}d^3\vec{r}\,' + V_{XC}[\rho(\vec{r})]\right]\psi_i(\vec{r}) = \varepsilon_i\psi_i(\vec{r}) \quad \text{(Eq 11)}$$

In the above equation, ε_i is the ith one-electron energy eigenvalue with $\psi_i(\vec{r})$ being the ith one-electron wavefunction. e is the electron charge, and ε_0 the vacuum permittivity. $-(\hbar^2/2m_e)\nabla^2$ represents the electronic kinetic energy with $\hbar = h/2\pi$ being the reduced Planck constant, m_e the electronic mass, and $\nabla^2 = \sum_{\alpha=1}^{3}\partial^2/\partial x_\alpha^2$ where x_α is the Cartesian coordinates of the electron. The term, $\frac{e^2}{4\pi\varepsilon_0}\sum_{I=1}^{N} Z_I/|\vec{r}-\vec{R}_I|$ represents the nuclear attraction potential with $\vec{r} = (x_1, x_2, x_3)$ and $\vec{R}_I$ the nuclear coordinates of the Ith atom of nuclear charge Z_I. The term, $e^2/4\pi\varepsilon_0\int(\rho(\vec{r}\,')/|\vec{r}-\vec{r}\,'|)d^3\vec{r}\,'$ represents the one-electron Hartree repulsion potential with $\rho(\vec{r})$ being the total electronic charge density. $V_{XC}[\rho(\vec{r})]$ represents the one-electron exchange-correlation potential and is given by the functional derivative:

$$V_{XC}[\rho(\vec{r})] = \frac{\delta}{\delta\rho(\vec{r})}E_{XC}[\rho(\vec{r})] \quad \text{(Eq 12)}$$

with $E_{XC}[\rho(\vec{r})]$ being the exchange correlation energy with the electron density of $\rho(\vec{r})$.

First-principles calculations have been used to study the ground state for a wide range of materials since all properties of a system are completely determined when the ground state electron density is known. The actual first-principles total energy calculations are performed in a self-consistent cycle. One first "guesses" the initial electron density, calculates the effective potentials, then solves the Kohn-Sham equations to determine a new electron density. This loop is repeated until the new electron density (or the new total energy) does not differ much from the old one, i.e., the ground state is reached. In practice, the nuclei also need to be relaxed into their equilibrium positions such that the quantum-mechanical forces acting on each of them vanish. Such structural relaxations are usually performed using a conjugate-gradient or a quasi-Newton scheme. There are three basic approaches in solving Kohn-Sham equations: plane wave and grid methods, localized atomic-like orbitals methods, and atomic spherical methods, with the last being the most general for precise solution of the Kohn-Sham equations. Furthermore, the total energy as a function of volume can be obtained by systematically carrying out the above calculations at volumes around that of the ground state, which is equivalent to compressing or expanding the solid. The equation of states (EOS) along with the bulk modulus and its derivative with respect to volume is generated by fitting the energy as a function of volume using various EOS models.

DFT-based first-principles calculations rely on the construction of cells of atomic structures with periodic boundary conditions. By solving Eq 11 for stoichiometric compounds and their respective constituents with given atomic structures, energies of formation of compounds can be obtained in a fairly straightforward manner with respect to those constituents at 0 K. For nonstoichiometric phases with various degrees of disordering, the periodic boundary conditions are destroyed, and the atomic positions are not completely fixed for given compositions. In principle, one could increase the number of atoms in cells to create supercells that adequately mimic the statistics of the random alloys and sample all possible atomic configurations, but it quickly becomes computationally prohibitive for practical calculations. As many physical properties can

be characterized by interactions between close neighbor atoms, Zunger and his colleagues[69,70] proposed the special periodic quasirandom structures (SQS) to mimic the correlation functions of the random solution for the first few shells around a given site, deferring errors due to periodicity to more distant neighbors. Different from other approaches in treating random solutions, the SQS method preserves all the features of DFT-based first-principles calculations.

The most challenging problem with the Kohn-Sham approach occurs when the electrons are not completely de-localized and interact strongly with each other such as in the rare-earth elements and their compounds. There are no existing exchange and correlation functionals to treat such systems properly. Various methods have been developed to improve the functionals when such effects are expected, including the "self-interaction correction" (SIC),[71] the LDA+U approach,[72] and the dynamic mean field theory (DMFT).[73] These nonlocal formulations remain active research areas of research.[74,75]

3.2 Multiscale Entropic Contributions

To calculate properties at finite temperatures, entropic contributions to the total energy need to be taken into account. Entropy is a measure of randomness in a system, and its microscopic definition in terms of statistic mechanics is based on the number of configurations of the system. In the field of materials science and engineering, three types of entropy are of interest, originating from three different scales:

(a) atomic scale in terms of mixing of species, commonly referred as configurational entropy;
(b) inter-atomic scale in terms of lattice vibrations, commonly referred as vibrational entropy; and
(c) electronic scale in terms of thermal excitation of electrons and spin polarizations, such as magnetic and ferroelectric polarizations.

Based on statistical thermodynamics, the three contributions can all be represented by a logarithmic measure of the DOSs, i.e.,

$$S = k_B \ln(w) \qquad \text{(Eq 13)}$$

where k_B is Boltzmann's constant and w the number of microstates for each case.

3.2.1 Atomic Scale: Mixing of Atoms. When the mixing between species is ideal, the number of microstates is $w = N!/\Pi N_i$ with N and N_i being the total number of atoms and the number of atoms of component i. The entropy of ideal mixing in terms of one mole of atom becomes

$$^{id}S_m^{mix} = -R\sum x_i \ln x_i \qquad \text{(Eq 14)}$$

where R is the gas constant and x_i the mole fraction of atom i. When the mixing is not ideal, short-range ordering develops. There are various approaches to treat short-range ordering. One of them is based on cluster expansion and Monte Carlo simulations.[76,77] In this approach, a microstate of atomic mixing is mapped into an Ising-like lattice model with each species represented by a spin (S_i). The total energy of any alloy configuration ($\sigma = <S_1, S_2,\ldots,S_n>$) can be conveniently calculated using the following Ising-like Hamiltonian:

$$E(\sigma) = J_0 + \sum_i J_i S_i + \sum_{i\neq j} J_{ij} S_i S_j + \sum_{i\neq j\neq k} J_{ijk} S_i S_j S_k + \cdots = \sum_f D_f J_f \overline{\Pi}_f \qquad \text{(Eq 15)}$$

In the above equation, Js are the effective cluster interactions (ECIs). Figures f are symmetry-related groupings of lattice sites with k vertices, e.g., single site, nearest-neighbor pair, three-body figures, etc., and span a maximum distance of m (m = 1, 2, 3… are the first, second, and third-nearest neighbors, etc.). D_f denotes the degeneracy factor of figure f. $\overline{\Pi}_f$ is the correlation function defined as the product of the spin variable over all sites of a figure, averaged over all symmetry-equivalent figures of the lattice. The advantage of the cluster expansion is that the energy converges rapidly with respect to the number of vertices. A sufficient accuracy for thermodynamic properties can be achieved by using relatively compact clusters, mainly short range pairs and small triplets. In systems where long-range elastic interactions are important, one may use a reciprocal-space formulation, equivalent to an infinite number of real space pair interactions.[78]

The ECIs of the cluster expansion are typically determined by a fit of the energy of a number of configurations from first-principles calculations. By subjecting the cluster expansions to Monte-Carlo simulations, the free energy of the system and thus the short-range ordering over the composition and temperature ranges can be efficiently obtained.

3.2.2 Inter-Atomic Scale: Lattice Vibration. At finite temperatures, atoms tend to fluctuate around their equilibrium lattice positions, resulting in lattice vibrations which can be represented by elastic waves made of phonons. Their energy is quantized proportional to the angular frequency of each elastic mode. Thermodynamic formulas can be derived on the basis of statistical mechanics from the phonon dispersion relation and summarized in terms of the phonon DOS giving the number of modes of oscillation as a function of frequency. In the Einstein model, each atom is assumed to vibrate independently. In a system with N atoms, there are 3 N independent harmonic oscillators with a common frequency, i.e., the phonon DOS with a single value. Alternatively in the Debye model, the lattice vibration is solved in the acoustic (low frequency) phonon branch with the upper limit characterized by the Debye frequency, which is directly related to the Debye temperature. Through the Debye-Grüneisen model,[79] the Debye temperature can be made volume-dependent based on the quasiharmonic approximation to account for anharmonicity.

In the commonly accepted lattice dynamics or phonon approach, first-principles calculations can be performed with either a harmonic or quasiharmonic approximation to obtain the full phonon spectra for a given atomic configuration. In these calculations, the restoring force constants tensors,

$\Phi(i,j)$, on atom i due to the displacement of atom j are computed from the second derivatives of the energy change with respect to the displacements. In a system with N atoms, the frequencies, v, of normal modes of oscillation between two atoms can then be obtained from the 3 N eigenvalues of the dynamical matrix of $\Phi(i,j)/\sqrt{M_i M_j}$ with M_i and M_j being the mass of atoms i and j. In the harmonic approximation, the vibrational entropy is obtained by summing up all microstates in terms of the vibrational phonon DOS, $g(v)$, as shown below[58,80]

$$S_{\text{vib}} = -k_{\text{B}} \int_0^\infty \ln\left[2\sinh\left(\frac{hv}{2k_{\text{B}}T}\right)\right] g(v)dv \qquad \text{(Eq 16)}$$

with h being Planck's constant.

There are two main approaches in determining the force constants: the linear response theory and the supercell method. In the linear response theory,[81] the dynamical matrix is directly evaluated in reciprocal space through the second-order change in energy due to atomic displacements from the perturbation theory. It thus accounts for infinite long-range force interactions and is accurate in the framework of DFT. In the supercell method, also known as the "frozen" phonon method, the calculations are more straightforward when compared to the linear response theory. In this method, the atoms are displaced slightly from their equilibrium positions, and the reaction forces are calculated. The displacements and reaction forces are then used to evaluate the force constants. Care must be taken in choosing the proper supercell sizes and the number of perturbations to ensure proper convergence of forces in addition to the energy.

One simple approach beyond the harmonic approximation is the so-called quasiharmonic approximation to account for thermal expansion and its effect on the vibrational properties. In the quasiharmonic approximation, the phonon DOS, $g(v)$, is made volume dependent by calculating the phonon DOS for several volumes within the harmonic approximation. The equilibrium volume at each temperature is then obtained by minimizing the free energy with respect to volume.

3.2.3 Electronic Scale: Thermal Electrons and Polarization. Two types of contributions in the electronic scale are discussed in this section: thermal electrons and spin polarization. The thermal electronic contribution becomes appreciable when the electronic DOS is high at the Fermi energy level. The bare electronic entropy S_{el} in the quasiharmonic approximation takes the form[58,82]

$$S_{\text{el}}(V,T) = -k_{\text{B}} \int n(\varepsilon, V)[f\ln f + (1-f)\ln(1-f)]d\varepsilon \qquad \text{(Eq 17)}$$

where $n(\varepsilon, V)$ is the electronic DOS with f being the Fermi distribution.

The recent treatment of magnetic spin polarization materials as a function of temperature[83] is based on the Heisenberg Hamiltonian in the mean-field and random-phase approximations with the exchange coefficients fitted to energy and polarization data from first-principles calculations. On the other hand, we developed a more straightforward approach by considering the magnetic state at finite temperatures being a mixture of various magnetic states competing with each other.[84,85] Assuming thermodynamic fluctuations happening locally, the partition function of a system under constant volume (V) and temperature (T), Z, is then written as

$$z = \sum Z^{\sigma} = \sum \exp\left(-\frac{F^{\sigma}(V,T)}{k_{\text{B}}T}\right) \qquad \text{(Eq 18)}$$

where σ labels the local electronic state, $F^{\sigma}(V,T)$ is the Helmholtz free energy for σ, Z^{σ} is the partition function for σ. The entropic contribution due to the different electronic states is obtained as[84,85]

$$S_{\text{conf}} = -k_{\text{B}} \sum x^{\sigma} \log x^{\sigma} \qquad \text{(Eq 19)}$$

with $x^{\sigma} = Z^{\sigma}/Z$ being the probability for finding electronic state σ. As a first-order of approximation, other properties of the mixture can be evaluated as a weighted average of those of individual states.

To predict the phase equilibrium behavior of ferroelectric materials as a function of temperature, Iniguez and Vanderbilt[86] used a first-principles effective-Hamiltonian approach[87] to carry out a theoretical study of the pressure-temperature phase diagram of $BaTiO_3$ with the path-integral quantum Monte Carlo technique to include quantum-mechanical fluctuations. The fundamental approximation is to use a low-order Taylor expansion to represent the energy surface based on the fact that the ferroelectric phase transition involves very small atomic displacements and strain deformations from the cubic structure. Based on our new approach for predicting magnetic transitions, it seems natural to consider the ferroelectric state at finite temperature as being a mixture of various ferroelectric states. We have thus developed a similar approach to calculate the pressure-temperature phase diagram of ferroelectric transitions, which is submitted for publication.

3.3 Ab Initio Molecular Dynamics Calculations

Molecular dynamics (MD) is a powerful tool to predict the thermodynamic and kinetic properties of solid, glass, and liquid phases. In MD simulations, atoms and molecules are allowed to interact for a period of time under Newton's second law or the equation of motion. If the force acting on each atom is known, it is possible to determine the acceleration of each atom in the system. Integration of the equations of motion then yields a trajectory that describes the positions, velocities, and accelerations of the atoms as they vary with time. Based on the position and velocity of each atom, the (statistical) average values of properties can be determined, including pressure, energy, diffusion coefficient, elastic constant, etc. Therefore, the key issue in MD simulations is the force acting on each atom. In classical molecular dynamics (CMD), empirical models are used to describe the force by considering bond, bend, and dihedral angle contributions with parameters fitted to experimental data or first-principles calculations of small clusters.

In the AIMD calculations proposed by Car and Parrinello,[88] the forces are calculated on the fly using the first-principles density functional theory as discussed above. They regarded the minimization of the Kohn-Sham functional as a minimization problem which can be solved by the MD-based simulated annealing method. In the work by Kresse and Hafner,[89] the minimization of the total energy is performed after each MD step. The DFT electronic wave functions are meaningful only when the electrons are in their ground state, and the atomic motion is described using Nosé dynamics[90,91] for closed systems at constant temperature and pressure. In addition to the issues facing DFT mentioned above, a recent review by Iftimie et al.[92] pointed out that the key challenges in the field of AIMD are the accuracy of the electronic structure method and the high computational overhead associated with the calculations. The former prevents accurate predictions of the total energy and the latter limiting the size of systems studied.

In addition to using AIMD in studying atomic configurations,[93,94] the quantitative calculations of phase equilibria using AIMD have been recently reported for pure Mo[95] and W,[34] showing great promise in accessing various structures which are unstable states at 0 K.

4. Integration of First-Principles Calculations and Entropies to CALPHAD Modeling

As mentioned in Section 2, there are two sets of input data used in the CALPHAD modeling: thermochemical data and phase equilibrium data. Thermochemical data is usually for individual phases and scarcer than phase equilibrium data which usually involves more than one phases and is relatively easier to obtain experimentally than thermochemical data. First-principles calculations thus complement experiments ideally by providing much needed thermochemical data of individual phases. In this section, we will briefly present our research results in the last few years in integrating first-principles calculations into the CALPHAD modeling through calculations at both 0 K and finite temperatures. In addition to thermodynamic properties, we have also used first-principles calculations to predict interfacial energy,[96] elastic coefficients,[97,98] and diffusion coefficients.[99] However, we did find that there are still significant discrepancies between the CALPHAD and first-principles lattice stability,[27] which hopefully will be resolved in the not-too-distant future. Nevertheless, the new capabilities derived from the integration of CALPHAD modeling and first-principles calculations based on quantum and statistic mechanics provide a new paradigm for enhanced predictability of physical property modeling as shown schematically in Fig. 5, and is particularly valuable for new materials with the dearth of experimental data.

4.1 Enthalpy of Formation at 0 K

When there are no phase transitions for the pure elements and compounds between 0 K and room temperature, the enthalpy of formation of a stable or metastable compound, Φ, can be approximated by the following equation

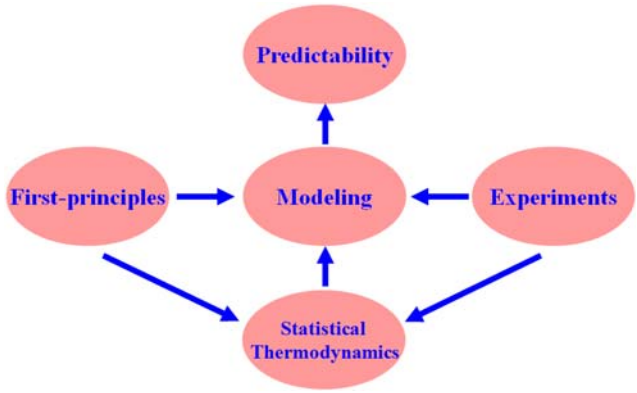

Fig. 5 A schematic diagram showing the integration of first-principles calculations, statistic thermodynamics, and CALPHAD modeling for enhanced predictability

$$\Delta H^{\Phi}(A_{1-x}B_x) \approx E^{\Phi}(A_{1-x}B_x) - (1-x)E^{\alpha}(A) - xE^{\beta}(B) \quad \text{(Eq 20)}$$

where E's are the first-principles calculated total energies of $A_{1-x}B_x$ in the structure Φ, and pure elements A and B in α and β structures, each fully relaxed to their equilibrium geometries. Calculated enthalpies of formation can significantly enhance the robustness of thermodynamic modeling and have been used in the following systems: Al-Sr,[100] Al-Ca,[101] Ni-Mo,[102] Al-Mg,[103] Co-Y,[104] Zn-Zr,[105] Mg-Al-Ca,[106] Ca-Mg,[107] Mg-Sr and Ca-Mg-Sr,[108] Hf-Si-O,[109] Al_2O_3-Nd_2O_3,[110] and Cu-Si.[111] In most cases, the first-principles calculations provided enthalpy of formation that was not previoulsy available in the literature. In some cases, such as Al-Sr, Al-Ca, Ni-Mo, and Cu-Si, the calculated data helps to define whether compounds are stable or not at low temperatures and to explore possible crystal structures observed in isoelectronic alloy systems. In the Al-Ca system, we compared the enthalpy of formation data from LDA and GGA using both an all-electron full-potential linearized augmented plane-wave method and an ultrasoft pseudopotential/plane wave method and found that they are in reasonable agreement with each other. For compounds with homogeneity ranges such as the *C14*, *C15*, and *C36* Laves phases, δ-NiMo, Co_5Y, and B_4C,[112] enthalpies of formation of their end-members were calculated and many of them were found to be positive, indicating that they are probably mechanically unstable at 0 K. This raises a concern with regard to the discrepancies between the CALPHAD and first-principles lattice stability of pure elements in fcc, bcc, and hcp structures.[27,30]

It should be pointed out that when there are phase transitions of pure elements between 0 K and room temperature, the above calculated enthalpy of formation at 0 K can no longer be directly compared with experimental data. To extend the first-principles calculations to finite temperatures, one faces the same challenge as in the case of unstable end-members because the high temperature phases

are usually mechanically unstable at 0 K. This prevents the calculations of phonon properties, an issue yet to be resolved.

4.2 Thermodynamics at Finite Temperatures

We have used both the linear response theory[58] and the supercell method[113] to predict the Helmholtz energy of Al, Ni, B_2-NiAl and $L1_2$-Ni_3Al by considering the phonon and thermal electronic contributions. With the deduced Helmholtz energy from phonon DOSs and electronic DOSs, the thermal expansion and enthalpy as a function of temperature were calculated and compared with the experimental data. Using the linear response theory,[58] our calculations show that the enthalpies of formation are slightly temperature dependent with a slope of −1.6 J/mol/K for B_2-NiAl and −1.2 J/mol/K for $L1_2$-Ni_3Al. For Ni, the inclusion of thermal electronic excitation results in a 10% increase in thermal expansion and 15% increase in enthalpy at 1600 K. In the supercell method, supercells with 8, 16, and 32 atoms were tested.[113] It was observed that with 32 atoms in the supercell, the phonon dispersion curves and the phonon DOSs from the linear response theory agree very well with the supercell method, along with the calculated thermodynamic properties.

We applied the supercell method to the Zn-Zr binary system.[114] From 0 K calculations, it was possible to find the likely ground state of the Zn_3Zr composition being $L1_2$ and to propose the observed high-temperature allotropic transformation of this phase to be from $L1_2$ to $D0_{23}$. From the convex hull construction, it was determined that $ZnZr_2$ and Zn_2Zr_3 are not part of the ground state of the Zn-Zr system. The vibrational properties of ZnZr, $ZnZr_2$ and Zn_2Zr_3 show that $ZnZr_2$ and Zn_2Zr_3 are dynamically stable at 0 K even though they did not belong to the ground state of the system. The resulting thermodynamic properties from the vibrational calculation indicate that $ZnZr_2$ and Zn_2Zr_3 could become stable with respect to the ZnZr + hcp two-phase field at elevated temperatures as shown in the CALPHAD modeling of the Zn-Zr system.[105] With these two phases stable at high temperatures, it was possible to resolve the discrepancies in the enthalpy of formation between the first-principles calculations and experimental data.

We have carried out phonon calculations for a number of systems including pure As[115] and B,[116] borides,[117] boron carbide,[112] ternary Al,[118] and Mg systems.[119] The predicted thermodynamic properties as a function of temperature compare well with experimental data when available. In the case of pure B, it is found that the defect-free α-B is more stable than the defect-free β-B at lower temperatures up to the predicted 1388 K, and the defect-free β-B is mechanically unstable at high temperatures (above 1840 K) indicated by the appearance of imaginary phonon modes. It was discovered that the instability can be suppressed by introducing defects, e.g., extra B atoms, consistent with the experimental observations that defects occur commonly in β-B. In pure As, an anomalous bonding with a considerable stretching force constant is found between atoms spanning alternate first and second nearest neighbors. This anomalous bonding, as a result of a Peierls distortion, is traceable from the undistorted simple cubic lattice exhibiting a giant Kohn anomaly at the R point. This is due to Fermi-surface nesting along the Γ-R direction, and stabilizes the layered A7 structure by suppressing the appearance of imaginary phonon modes.

In the Ca-Sn system, the first-principles result for the formation energy of the dominating Ca_2Sn intermetallic phase at 298 K is less exothermic by a factor of 1.6 compared to the experimental values.[119] We thus performed two types of thermodynamic modeling: one based on the first-principles output and the other based on the experimental data.[120] Both models describe the phase diagram with quite high accuracy. In the first-principles modeling, the Gibbs energies of the intermetallic compounds were fully quantified from the first-principles finite temperature properties, and the superiority of this thermodynamic description is demonstrated. On the other hand, when the experimental enthalpy of formation is used, the absolute entropies of the Ca-rich intermetallic phases do not only deviate drastically from the room temperature calculated first-principles data, but also lead to unrealistically large entropies of formation of the intermetallic phases and the enthalpy of mixing of the liquid. It is shown that it is the combination of finite temperature first-principle calculations and the tool of the CALPHAD modeling that provides a sound basis to identify and decide on conflicting key thermodynamic data in the Ca-Sn system. The decision made for the enthalpy of formation of Ca_2Sn is also of the utmost importance for calculations in multicomponent Ca-Sn-Mg alloy systems, such as the extension of the Ca_2Sn liquidus surface and other equilibria involving this dominating phase.[121]

In the ternary Al-Ni-Y system, ten ternary compounds were investigated[118] using the quasi-harmonic approximation to obtain both enthalpy and entropy of formation. They are used in the prediction of the Al-rich region of the Al-Co-Ni-Y system, resulting in good agreement between phase fractions from the Scheil simulation when compared with experimentally determined data for three Al-rich quaternary alloys.[122]

4.3 Magnetic Property and Magnetic Transition

In an effort to understand the effects of rare-earth elements on the properties of Mg alloys, we encountered two challenges in predicting the thermodynamic property of Ce as a function of temperature: the strongly correlated *f* electrons and complex magnetic transitions of fcc Ce between 0 K and room temperature with an intermediate double-hcp phase. We used the GGA + U approach to treat the strong correlations in Ce.[84] Evaluation of numerous U-J values over a 1.0-6.0 eV range revealed that 1.6 eV gives the most consistent prediction of nonmagnetic Ce (α-Ce) and magnetic Ce (γ-Ce) energetics over the range of atomic volumes that includes both phases. Alternatively, for U − J = ∼1.7 eV, the computed 0 K energy of magnetic Ce is comparable to that of nonmagnetic Ce which is implausible since γ-Ce is not stable at 0 K. Values of U − J larger than 1.7 eV were precluded from consideration since magnetic Ce is lower in energy than nonmagnetic Ce at 0 K. Using U − J = 1.6 eV, the individual Helmholtz energies of α-Ce and γ-Ce are calculated as a function of temperature

and volume using Eq 10 with both phonon and thermal electronic contributions included. The magnetic contribution to γ-Ce due to spin disordering was taken into account by the generalized Hund's rule.

We consider that the state of the system at finite temperatures and pressures/volumes is a mixture of the two states of α-Ce and γ-Ce and can be represented by the partition function of the system in terms of Eq 18 and the corresponding Helmholtz energy as $F(V,T) = -k_B T \log Z$. By minimizing $F(V,T)$ with respect to volume for given temperatures, the equilibrium state of the system is obtained. The temperature-volume/pressure phase diagrams and the EOS between volume and pressure are predicted with remarkable agreement when compared to available experimental data. It is predicted that the α-Ce to γ-Ce transition is first-order at low temperatures and second-order at high temperatures. The predicted critical point is at T_c = 476 K and P_c = 2.22 GPa in agreement with experimental data from several groups. This is analogous to the miscibility gap, common in binary alloy systems,[123,124] which can also be induced by magnetic transitions.[125,126] It should be mentioned that the two phases in equilibrium at low temperatures are no longer pure nonmagnetic α-Ce and ferromagnetic γ-Ce, but mixtures of both states at the same volume with one being dominant in one phase and the other being dominant in the other phase. With the increase of temperature, the fraction of the minor state increases until the critical point is reached where the two states have equal contributions. Beyond the critical point, the two phases become undistinguishable and change their properties continuously with temperature and pressure. Since each phase is a mixture of two states with the same volume, the miscibility gap in our calculation represents a coherent miscibility gap residing in the incoherent miscibility gap,[124] and both are shown in the publication.[84] The rather scattered experimental data of the phase boundary may reflect the different degree of coherency during the phase transition. At 300 K, we predict a 5.36 Å^3 $\gamma \rightarrow \alpha$ volume collapse ($V_\gamma - V_\alpha$) which is in excellent agreement with the experimental values of ~4.8 and ~5.0 Å^3. Furthermore, with the system's Helmholtz energy available, the heat capacity can be obtained and is shown in Fig. 6 for a second-order magnetic transition as a function of temperature at 2.25 GPa, slightly above the pressure of the critical point.

It is self-evident from Eq 18 that more states are desirable, particularly those between the two extreme states of pure nonmagnetic α-Ce and ferromagnetic γ-Ce. Consequently, we have included an antiferromagnetic state with energy between the nonmagnetic and ferromagnetic states,[85] which gives similar macroscopic thermodynamic properties, but with more microscopic details. We have further developed approaches to calculate magnetization and heat capacity as a function of temperature and pressure.

4.4 Enthalpy of Mixing in Binary and Ternary Substitutional Solutions

In our research activities, we have focused on using SQS to obtain the enthalpy of mixing in fcc, bcc, and hcp

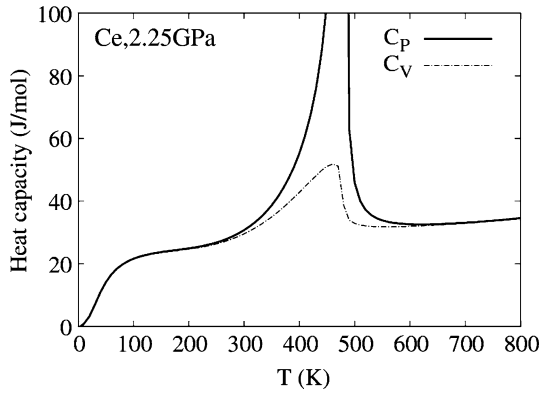

Fig. 6 Predicted heat capacity for second-order magnetic transition of Ce as a function of temperature at 2.25 GPa pressure, slightly above the critical pressure[151]

solutions. Based on the SQS supercells for binary fcc solutions,[70] we developed the SQS supercells for binary bcc,[127] binary hcp,[128] and ternary fcc solutions.[129] The SQS for ternary bcc and hcp solutions are also developed and will be published shortly.[130] For compounds with homogeneity ranges, the SQS approach can be applied to individual sublattices as shown for B2,[131] Laves C14, C15, and C36 phases,[36] $L1_2$,[132] and halite.[133]

For perfectly random solutions, there is no correlation in the occupation between various sites, and therefore correlation function, $\overline{\Pi}_{k,m}$ for figures with k vertices and a distance of m such as single site, nearest-neighbor pair, three-body figures etc., simply becomes the product of the lattice-averaged site variable, which is related to the composition. The SQS approach aims to find small-unit-cell ordered structures that possess $\left(\overline{\Pi}_{k,m}\right)_{SQS} \cong \left\langle \overline{\Pi}_{k,m} \right\rangle_{Random}$ for as many figures as possible. For random $A_{1-x}B_x$ bcc substitutional alloys, the correlation function is $\overline{\Pi}_{k,m} = (2x-1)^k$. The 2-, 4-, 8-, and 16-atoms SQS supercells[127] were generated using the alloy-theoretic automated toolkit (ATAT),[134] respectively, for x = 0.5 and 0.25. By switching the A and B atom positions for the supercell with x = 0.25, one obtains the SQS for x = 0.75. The 16-atom SQS supercells closely mimic the most relevant pair and multisite correlation functions of random solutions. Those SQS supercells were tested in the Mo-Nb, Ta-W, and Cr-Fe systems, where the bcc structure is known to be stable over the whole composition range. The predicted formation enthalpies, equilibrium lattice parameters, and magnetic moments of those bcc alloys agree satisfactorily with most existing experimental data in the literature. The magnetic effects are found to be significant in Cr-Fe. It is observed that even in perfectly lattice-mismatched systems such as Cr-Fe, the average A-A, A-B, and B-B bond lengths can be quite different.

For random $A_{1-x}B_x$ hcp substitutional alloys, the correlation function is the same as the bcc solutions, i.e., $\overline{\Pi}_{k,m} = (2x-1)^k$. For simplicity, the ideal c/a ratio was used to generate SQS supercells with 8 and 16 atoms.[128] It should be mentioned that the order of a given figure may be

altered with the variation of c/a ratio, e.g., changing from second nearest neighbor to third nearest neighbor, but it will not cause changes in the values of the correlation functions. Since there are two atomic sites in the hcp primitive cell, some figures have more than one crystallographically nonequivalent figure at the same distance. For example, the two pairs (0, 0, 0) and (a, 0, 0); (0, 0, 0) and (1/3, 2/3, 1/2), have the same inter-atomic distance, a, but they do not share the same symmetry operations. This degeneracy is broken when the c/a ratio deviates from its ideal value. Furthermore, in the hcp structure for a given range of correlations, there are more symmetrically distinct correlations to match than those in fcc and bcc and many more candidate configurations to search through in order to find a satisfactory SQS supercell. Seven binary systems, Cd-Mg, Mg-Zr, Al-Mg, Mo-Ru, Hf-Ti, Hf-Zr, and Ti-Zr, were studied to test the hcp $A_{1-x}B_x$ SQS supercells for $x = 0.25$, 0.5, and 0.75. The radial distribution analysis for characterizing local relaxation of the fully relaxed SQS supercells, bond length, lattice parameters, and enthalpy of mixing were obtained and compared with available experimental observations. It was demonstrated that care must be taken to ensure that the fully relaxed SQS maintain the hcp symmetry.

For binary systems, conventional values of the site occupation variables in terms of the Ising model are ± 1 depending on whether a lattice site is occupied by A or B atoms. In ternary systems, the site occupation variables take +1, 0, or −1 if a lattice site is occupied by A, B, or C atoms, respectively. The correlation functions of a random substitutional solution can then be evaluated and used in generating the SQS supercells at the equimolar composition where $x_A = x_B = x_C = 1/3$ and at $x_A = 1/2$, $x_B = x_C = 1/4$. By switching the occupation of the A atoms in the second SQS supercell with either B or C atoms, two other SQS supercells can be obtained where $x_A = 1/4$, $x_B = 1/2$, $x_C = 1/4$ and $x_A = x_B = 1/4$, $x_C = 1/2$. Therefore, the enthalpy of mixing at four different compositions in a ternary system can be determined. Seven SQS supercells with 4 to 64 atoms were generated. When the number of atoms in the ternary SQS supercells was fewer than 24, ATAT[134] was used to generate ternary fcc SQSs. The time needed to find SQS supercells increases exponentially with the size of a supercell because ATAT enumerates all the atomic configurations in checking the correlation functions. Therefore, a Monte Carlo-like scheme was used for supercells with more than 24 atoms. The Ca-Sr-Yb system was studied along with its constitutive binary systems.[129] The calculated ternary enthalpies of mixing are compared with the data extrapolated from the binaries based on Eq 8 with the latter being slightly lower. This is supported by the observation that first-principles calculations of all the binary and ternary SQS supercells in the Ca-Sr-Yb system exhibit very small local relaxation. It was also observed that the enthalpies of mixing in fcc and bcc solutions are very similar to each other, and they are all positive as is the experimental enthalpy of mixing in the liquid.

The ternary fcc SQS supercells were also applied to Al-Cu-Mg, Al-Cu-Si, and Al-Mg-Si systems.[135] In the Al-Cu-Mg and Al-Mg-Si systems, the ternary SQS enthalpies of formation agree well with the extrapolated enthalpies of mixing for one set of binary systems, indicating weak ternary interactions and that no ternary interaction parameters are needed with those binary data. On the other hand, there are significant differences with the COST507 database.[136] In the Al-Cu-Mg system, the incorrect enthalpy of mixing in the fcc Cu-Mg system is found, while in the Al-Mg-Si system, the enthalpies of mixing in the Al-Si and Mg-Si systems in the COST507 database are considerably less negative than those in the other literature and the first-principles calculations. In the Al-Cu-Si system, the mixing enthalpies for the fcc phase from the COST507 database and the combined three binaries from the literature are close to each other. However, both are several kJ lower than the values from the first-principles calculations of ternary fcc SQS, indicating that positive ternary interaction parameters are needed. This is due to the Al addition weakening the strong Cu-Si interaction, while the Cu addition tends to be ordered with both Si and Al.

SQS calculations have been systematically applied in the CALPHAD modeling of a number of systems, including Ni-Mo,[102] Mg-Zr,[137] Al-Mg,[103] Zn-Zr,[105] K-Na and KF-NaF,[133] Ca-Mg,[107] Ba-Ni and Ba-Ti,[138] Ca-Ce,[139] and Cu-Si.[111]

4.5 Defect Structure and Lattice Preference

The study of point defects in terms of first-principles calculations is usually carried out by introducing one defect in a given supercell such as the formation of a vacancy. In our work related to the prediction of diffusion coefficients, the enthalpy and entropy of vacancy formation in a range of fcc, bcc, and hcp elements were calculated,[99,140] showing good agreement with available experimental data. To investigate the effects of a high concentration of point defects, the SQS approach can be used. Our research has been focused on the B2 structure by developing SQS supercells for random $A_{1-x}B_xC$ B2 alloys with A and B randomly distributed on one B2 sublattice and the second sublattice completely occupied by C, so the substitutional alloy problem is thus simple-cubic-based.[131] As an example, the atomic structure of a SQS B2 $A_{0.75}B_{0.25}C$ with total 32 atoms is shown in Fig. 7.[131] Switching the A and B atoms results in a SQS of $A_{0.25}B_{0.75}C$. For B2 NiAl, defects treated include Ni vacancies (Va), Al vacancies, Ni antisites and Al antisites as $Ni_{1-x}Va_xAl$, $Al_{1-x}Va_xNi$, $Al_{1-x}Ni_xNi$, and $Ni_{1-x}Al_xAl$ pseudobinary B2 alloys at compositions $x = 0.25$ and 0.5, respectively. The predicted formation enthalpies, equilibrium lattice parameters, and elastic constants of nonstoichiometric B2 NiAl are in satisfactory agreement with experimental data in the literature. Our calculations unambiguously show that Ni vacancies and Ni antisites are the constitutional point defects in Al-rich and Ni-rich B2 NiAl, respectively, even at high defect concentrations. A structural instability of B2 NiAl induced by Ni antisites was predicted, which coincides with the occurrence of a martensitic transformation in this compound at high Ni concentrations.[131]

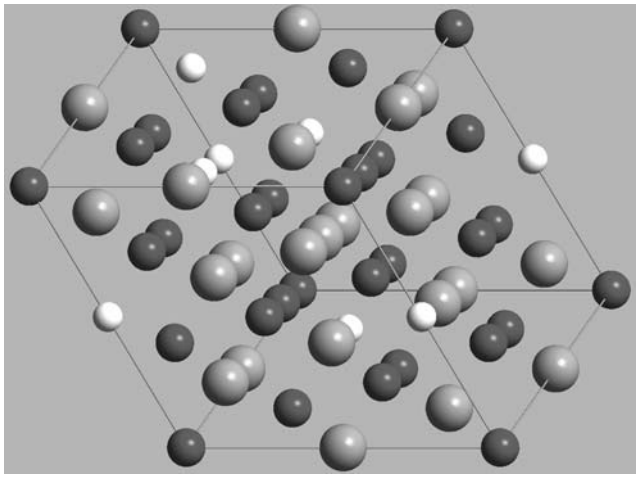

Fig. 7 Atomic structure of a SQS for B2 $(A_{0.75}B_{0.25})C$ with A in gray, B in white, and C in black, and total 32 atoms[131]

In B2 PdIn, our calculations show that Pd vacancies and Pd antisites are the constitutional point defects in In-rich and Pd-rich B2 PdIn, respectively.[141] Furthermore, our results suggest that the predominant thermal defects in B2 PdIn are of triple-Pd type and not of Schottky type. Unlike B2 NiAl, in which the thermal defects are of triple-defect type on the Ni-rich side and of interbranch type on the Al-rich side,[142] the thermal defects in B2 PdIn are of triple-defect type on both sides of stoichiometry. Utilizing the statistical-mechanical Wagner-Schottky model, the predicted vacancy concentrations are in satisfactory agreement with existing experimental data in the literature.

In B2 RuAl, the dominant composition conserving constitutional defect structures have been determined as Ru vacancies and Al antisites in the Al-rich side with a high energy penalty for any defects in the Ru-rich side.[143] In the ternary B2 NiRuAl, it was observed that Ru prefers the Ni-sublattice in NiAl, while Ni has a very strong preference for the Ru-sublattice in RuAl. Furthermore, the enthalpies of formation of the complex composition-conserving defect structures due to the ternary element addition with respect to B2 NiAl and B2 RuAl indicate that a miscibility gap is likely to be stable at low temperatures in the NiAl-RuAl pseudobinary system.[143]

In studying the defects in β-boron, the force constants and phonon dispersion relations are calculated at equilibrium and larger than equilibrium volumes.[116] The most unusual decrease of the force constant with increasing volume is found in one of the stretching terms, caused by the significant increase of the nearest bond length. Figure 8 plots the charge density contours around the hexagonal ring a-b-c-d-e-f with a-b, c-d, and e-f being the nearest neighbors in the icosahedra in β-boron.[116] It clearly demonstrates the significant decrease of the charge density between the nearest neighbors. Phonon calculations at several volumes indicate that the imaginary phonon modes in the defect-free β-boron occur with V/V_0 larger than 1.067 (pertaining to temperatures above 1840 K). It is thus expected that the appearance of imaginary phonon modes can be suppressed

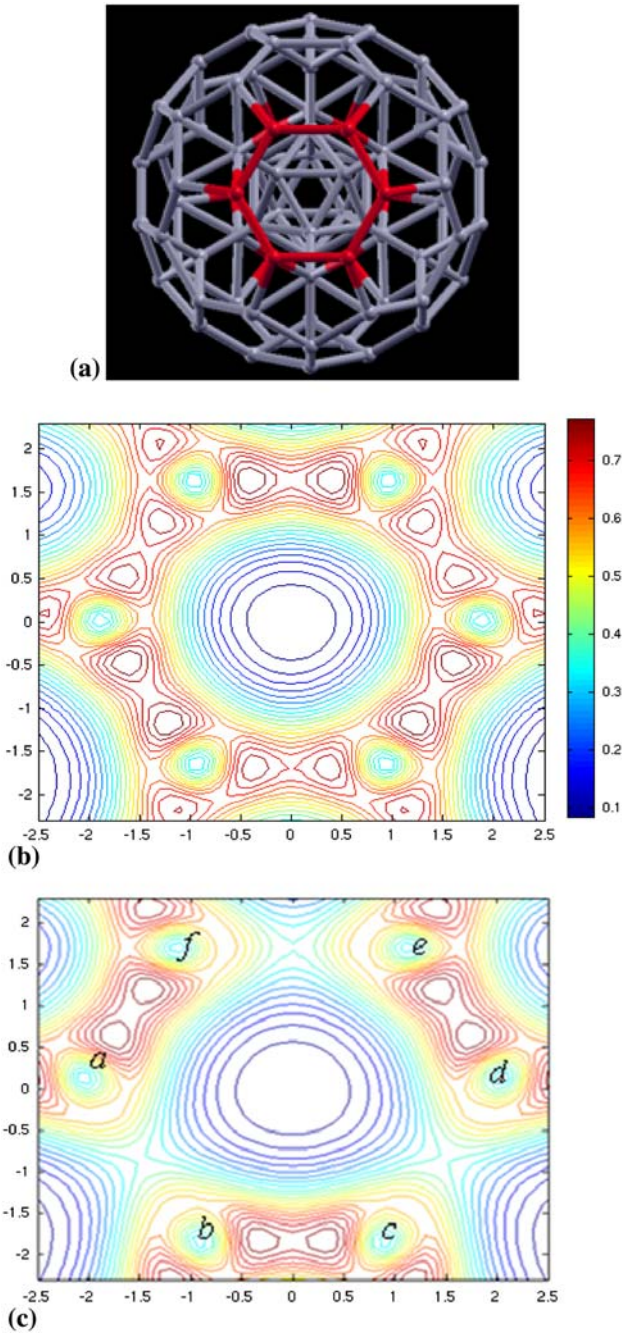

Fig. 8 Charge density contours around the hexagonal ring linking the icosahedra in β-boron (a), at equilibrium volume (b), and 1.125 of the equilibrium volume (c)[116]

by introducing defects. Phonon calculations with extra B atoms added to the weak bonding locations indicate that (i) the largest negative stretching force constant increases and is close to zero; (ii) the values of imaginary phonon modes increase. Therefore, the presence of extra B atoms hinders the bond cleavage. These are in agreement with the analysis of the charge density distributions showing that the maximum charge densities shift to the inner part of the B

hexagonal ring, implying the glue-like effect of the extra B atoms.

4.6 Structure of Liquid, Super-Cooled Liquid, and Glass

Quantitative prediction of thermodynamic properties of the liquid phase from first-principles remains to be a challenging task due to the significant uncertainty of its atomic arrangements. AIMD has emerged as a promising approach in studying the structure and properties of liquid, super-cooled liquid, and glass phases as mentioned in a previous section of this paper. We started by examining the structural evolution of Cu[144] and Zr[145] during two rapid quenching processes from 1500 K for Cu and 2200 K for Zr, i.e., a direct quenching of 2.0×10^{14} K/s and a stepwise quenching with 1000 time steps (about 5 ps) at every 200 to 300 K temperature interval until room temperature, resulting in an average quenching rate of 4.0×10^{13} K/s. Between two temperatures in the stepwise quenching, the system is quenched at a rate of 1 K per time step as in the direct quenching approach. Internal energy, pair-correlation functions, and bond pairs as a function of temperature were characterized for both quenching processes.

The AIMD predicted pair correlation functions of Cu at 1500 K agree well with experimentally measured data even for the second and third peaks. Good agreement is also seen with the self-diffusion coefficient $D = 4.0 \pm 0.5\times10^{-9}$ m^2/s at 1500 K from the mean square displacement, very close to the experimental value of $D = 3.97\times10^{-9}$ m^2/s at 1358 K,[146] which validates the AIMD approach.[144] Under stepwise quenching, liquid Cu transforms to the fcc phase at about 600 K as evidenced by an internal energy jump, abrupt changes in pair correlation functions in the shape of the second and third peaks and several small new peaks around them, significant increase of bond pairs corresponding to fcc and hcp structures, and near-zero mean square displacement. While in direct quenching, the liquid Cu is frozen into a glass state by about 800 K with a clear change in the slope of energy to temperature. However, there is no energy jump, no abrupt change in pair correlation functions, and there is partial transformation of part of icosahedral clusters to bcc clusters. It also reveals that icosahedral and tetrahedral clusters are predominant in the liquid state, while the icosahedral, bcc, and tetrahedral clusters are predominate in the glass state. Icosahedral and bcc SRO are significantly enhanced during the liquid-glass quenching process, whereas tetrahedral SRO is slightly decreased. In the case of Zr, it is shown that liquid Zr transforms to a metastable bcc phase (β-Zr) about 1000 K as quenched at the rate of 4.3×10^{13} K/s.[145] When quenched at 2.0×10^{14} K/s, however, the crystallization is suppressed and liquid Zr is frozen into a glass phase. Bond pair analysis reveals that short range order in both states mostly consists of icosahedral and bcc clusters.

We have extended the AIMD calculations to several families of bulk metallic glasses, including CuZrAl,[147] MgCuY,[93,148] and ZrTiCuNiBe alloys.[94,149,150] It is clear to the author that the great potential of the AIMD approach is yet to be discovered.

5. Summary

In this overview, the fundamentals, approximations, and applications of first-principles calculations and the CALPHAD modeling are presented with an emphasis on the integration of the two approaches. It is demonstrated that the thermodynamic, kinetic, and structural properties at finite temperatures predicted from first-principles calculations and multiscale entropic contributions based on the first-principles calculations not only extend our deeper understanding of alloy theories, but also provide quantitative inputs in the CALPHAD modeling of a wide range of materials properties. The power of integrating first-principles calculations and the CALPHAD modeling is significant to the development of robust materials databases and will become even more important as the capabilities of first-principle calculations continue to develop. With an increasing amount of data from first-principles calculations that was not available before, the CALPHAD modeling procedures are also changing. For example, in the last few years, we have been working on developing frameworks for automatic updating of multicomponent thermodynamic databases using data from first-principles calculations to reduce uncertainties in model parameters.[152]

Acknowledgments

The author greatly appreciates the support from National Science Foundation under grants 9983532 (CAREER), 0073836, 0205232, 0209624, 0510180, 0514592, and 0541674, Department of Energy through the grant DE-ED1803000, the United States Automotive Materials Partnership (USAMP) of Department of Energy through cooperative agreement No. DE-FC05-02OR22910, Office of Naval Research for the grant N0014-07-1-0638, and US Army Research Laboratory for the grant W911NF-08-2-0064. The author would also like to thank the students and research fellows at the Phases Research Lab at Penn State for their diligent work, particularly those whose publications are cited in the paper, i.e., Raymundo Arroyave, Carl Brubaker, Swetha Ganeshan, William Golumbfskie, Takayuki Honda, Chao Jiang, Manjeera Mantina, Koray Ozturk, Sara Prins, James Saal, Shun Li Shang, Dongwon Shin, Tao Wang, Yi Wang, Mei Yang, Hui Zhang, Shengjun Zhang, Yu Zhong, and Shihuai Zhou. It should be mentioned that Prof. Jorge Sofo, Dr. Yi Wang, Dr. Shun Li Shang, and Dr. Raymundo Arroyave have been instrumental in developing our expertise in first-principles calculations. The author is grateful for opportunities to collaborate with many colleagues at the Pennsylvania State University and other universities in the US and China as evidenced in the references cited. Particularly, the long-term collaborations with Prof. Long-Qing Chen at the Pennsylvania State University, Prof. Chris Wolverton at Northwestern University, Dr. Alan Luo from General Motor Company, and Prof. Xidong Hui from University of Science and Technology Beijing (USTB) have been very enjoyable and fruitful. The author thanks Ms. Chelsey Zacherl for her careful reading of the manuscript.

References

1. Z.K. Liu, L.Q. Chen, R. Raghavan, Q. Du, J.O. Sofo, S.A. Langer, and C. Wolverton, An Integrated Framework for Multi-Scale Materials Simulation and Design, *J. Comput-Aided Mater. Des.*, 2004, **11**, p 183-199
2. Z.K. Liu and L.-Q. Chen, Integration of First-Principles Calculations, Calphad Modeling, and Phase-Field Simulations, *Applied Computational Materials Modeling: Theory, Experiment and Simulations*, G. Bozzolo, Ed., Springer, Berlin, 2006,
3. Z.K. Liu and D.L. McDowell, Center for Computational Materials Design (CCMD) and Its Education Vision, *Fundamentals and Characterization, Vol 1: Materials Science and Technology (MS&T) 2006*, B. Fahrenholtz, A. Kimel, and P.E. Cantonwine, Ed., Cincinnati, OH, 2006, p 111-118
4. Z.K. Liu, The Minerals, Metals & Materials Society, *Integrating Forward Simulation and Inverse Design of Materials*, http://iweb.tms.org/Purchase/ProductDetail.aspx?Product_code=WEB-07-7063, 2009
5. L. Kaufman, Computational Thermodynamics and Materials Design, *CALPHAD*, 2001, **25**, p 141-161
6. P.J. Spencer, A brief history of CALPHAD, *CALPHAD*, 2008, **32**, p 1-8
7. L. Kaufman, The Lattice Stability of Metals.1. Titanium and Zirconium, *Acta Metall.*, 1959, **7**, p 575-587
8. L. Kaufman, The Lattice Stability of the Transition Metal, *Phase Stability in Metals and Alloys*, P.S. Rudman, J.S. Stringer, and R.I. Jaffee, Ed., McGraw-Hill, New York, 1967, p 125-150
9. L. Kaufman, Stability of Metallic Phases, *Prog. Mater. Sci.*, 1969, **14**, p 55
10. L. Kaufman and H. Bernstein, *Computer Calculation of Phase Diagram*, Academic Press Inc., New York, 1970
11. J. Agren, Numerical Treatment of Diffusional Reactions in Multicomponent Alloys, *J. Phys. Chem. Solids*, 1982, **43**, p 385-391
12. J.O. Andersson and J. Agren, Models for Numerical Treatment of Multicomponent Diffusion in Simple Phases, *J. Appl. Phys.*, 1992, **72**, p 1350-1355
13. X.G. Lu, M. Selleby, and B. Sundman, Implementation of a new model for pressure dependence of condensed phases in Thermo-Calc, *CALPHAD*, 2005, **29**, p 49-55
14. B. Hallstedt, N. Dupin, M. Hillert, L. Hoglund, H.L. Lukas, J.C. Schuster, and N. Solak, Thermodynamic Models for Crystalline Phases. Composition Dependent Models for Volume, Bulk Modulus and Thermal Expansion, *CALPHAD*, 2007, **31**, p 28-37
15. W. Hume-Rothery, Factors Affecting the Stability of Metallic Phases, *Phase Stability in Metals and Alloys*, P.S. Rudman, J.S. Stringer, and R.I. Jaffee, Ed., McGraw-Hill, New York, 1967, p 3-23
16. L. Brewer, Viewpoints of Stability of Metallic Structures, *Phase Stability in Metals and Alloys*, P.S. Rudman, J.S. Stringer, and R.I. Jaffee, Ed., McGraw-Hill, New York, 1967, p 39-62
17. D.G. Pettifor, Physicists View of Energetics of Transition-Metals, *CALPHAD*, 1977, **1**, p 305-324
18. J. Hafner and F. Sommer, Ab Initio Pseudopotential Calculations of Structure and Stability of Binary-Alloys and Intermetallic Compounds, *CALPHAD*, 1977, **1**, p 325-340
19. A.R. Miedema, F.R. Deboer, and R. Boom, Model Predictions for Enthalpy of Formation of Transition-Metal Alloys, *CALPHAD*, 1977, **1**, p 341-359
20. E.S. Machlin, Modified Pair Potentials and Alloy Phase-Stability, *CALPHAD*, 1977, **1**, p 361-377
21. J.O. Andersson, A.F. Guillermet, P. Gustafson, M. Hillert, B. Jansson, B. Jonsson, B. Sundman, and J. Agren, A New Method of Describing Lattice Stabilities, *CALPHAD*, 1987, **11**, p 93-98
22. N. Saunders, A.P. Miodownik, and A.T. Dinsdale, Metastable Lattice Stabilities for the Elements, *CALPHAD*, 1988, **12**, p 351-374
23. Y.A. Chang, C. Colinet, M. Hillert, Z. Moser, J.M. Sanchez, N. Saunders, R.E. Watson, and A. Kussmaul, GROUP 3: Estimation of Enthalpies for Stable and Metastable States, *CALPHAD*, 1995, **19**, p 481-498
24. B.P. Burton, N. Dupin, S.G. Fries, G. Grimvall, A.F. Guillermet, P. Miodownik, W.A. Oates, and V. Vinograd, Using Ab Initio Calculations in the CALPHAD Environment, *Z. Metallk.*, 2001, **92**, p 514-525
25. P.E.A. Turchi, I.A. Abrikosov, B. Burton, S.G. Fries, G. Grimvalle, L. Kaufman, P. Korzhavyi, V.R. Manga, M. Ohno, A. Pisch, A. Scott, and W.Q. Zhang, Interface Between Quantum-Mechanical-Based Approaches, Experiments, and CALPHAD Methodology, *CALPHAD*, 2007, **31**, p 4-27
26. H.L. Skriver, Crystal-Structure from One-Electron Theory, *Phys. Rev. B*, 1985, **31**, p 1909-1923
27. Y. Wang, S. Curtarolo, C. Jiang, R. Arroyave, T. Wang, G. Ceder, L.Q. Chen, and Z.K. Liu, Ab Initio Lattice Stability in Comparison with CALPHAD Lattice Stability, *CALPHAD*, 2004, **28**, p 79-90
28. S. Curtarolo, D. Morgan, and G. Ceder, Accuracy of Ab Initio Methods in Predicting the Crystal Structures of Metals: A Review of 80 Binary Alloys, *CALPHAD*, 2005, **29**, p 163-211
29. L. Kaufman, CALPHAD: Computer Coupling of Phase Diagrams and Thermochemistry—Foreword, *CALPHAD*, 2002, **26**, p 141
30. G. Grimvall, Reconciling Ab Initio and Semiempirical Approaches to Lattice Stabilities, *Ber. Bunsen-Ges. Phys. Chem. Chem. Phys.*, 1998, **102**, p 1083-1087
31. A.E. Kissavos, S. Shallcross, V. Meded, L. Kaufman, and I.A. Abrikosov, A Critical Test of Ab Initio and CALPHAD Methods: The Structural Energy Difference Between bcc and hcp Molybdenum, *CALPHAD*, 2005, **29**, p 17-23
32. C. Asker, A.B. Belonoshko, A.S. Mikhaylushkin, and I.A. Abrikosov, First-Principles Solution to the Problem of Mo Lattice Stability, *Phys. Rev. B*, 2008, **77**, p 220102
33. G. Grimvall, Extrapolative Procedures in Modelling and Simulations: The Role of Instabilities, *Sci. Model. Simul.*, 2008, **15**, p 5-20
34. V. Ozolins, First-Principles Calculations of Free Energies of Unstable Phases: The Case of fcc W, *Phys. Rev. Lett.*, 2009, **102**, p 065702
35. S.G. Fries and B. Sundman, Using Re-W Sigma-Phase First-Principles Results in the Bragg-Williams Approximation to Calculate Finite-Temperature Thermodynamic Properties, *Phys. Rev. B*, 2002, **66**, p 012203
36. Y. Zhong, A.A. Luo, J.O. Sofo, and Z.K. Liu, First-Principles Investigation of Laves Phases in Mg-Al-Ca System, *Mater. Sci. Forum*, 2005, **488-489**, p 169-175
37. M.C. Gao, A.D. Rollett, and M. Widom, First-Principles Calculation of Lattice Stability of C15-M2R and Their Hypothetical C15 Variants (M = Al, Co, Ni; R = Ca, Ce, Nd, Y), *CALPHAD*, 2006, **30**, p 341-348
38. M.H.F. Sluiter, Ab Initio Lattice Stabilities of Some Elemental Complex Structures, *CALPHAD*, 2006, **30**, p 357-366
39. M. Šob, A. Kroupa, J. Pavlu, and J. Vreštál, Application of Ab Initio Electronic Structure Calculations in Construction of Phase Diagrams of Metallic Systems with Complex Phases, *Solid State Phenom*, 2009, **150**, p 1-29

40. N. Saunders and A.P. Miodownik, *CALPHAD (Calculation of Phase Diagrams): A Comprehensive Guide*, Pergamon, Oxford, New York, 1998
41. H.L. Lukas, S.G. Fries, and B. Sundman, *Computational Thermodynamics: The CALPHAD Method*, Cambridge University Press, New York, 2007
42. M. Hillert, *Phase Equilibria, Phase Diagrams and Phase Transformations*, 2nd ed., Cambridge University Press, Cambridge, 2007
43. M. Hillert and L.I. Stafansson, Regular Solution Model for Stoichiometric Phases and Ionic Melts, *Acta Chem. Scand.*, 1970, **24**, p 3618
44. M. Hillert, The compound energy formalism, *J. Alloy. Compd.*, 2001, **320**, p 161-176
45. A.D. Pelton and M. Blander, Thermodynamic Analysis of Ordered Liquid Solutions by a Modified Quasi-Chemical Approach—Application to Silicate Slags, *Metall. Mater. Trans. B*, 1986, **17**, p 805-815
46. A.D. Pelton, M. Blander, M.T. ClavagueraMora, M. Hoch, L. Hoglund, H.L. Lukas, P. Spencer, and B. Sundman, Thermodynamic Modeling of Solutions and Alloys—Schloss Ringberg, March 10-16, 1996—Group 1: Liquids, *CALPHAD*, 1997, **21**, p 155-170
47. A.D. Pelton and P. Chartrand, The Modified Quasi-Chemical Model: Part II. Multicomponent Solutions, *Metall. Mater. Trans. A*, 2001, **32**, p 1355-1360
48. W.A. Oates, F. Zhang, S.L. Chen, and Y.A. Chang, Improved Cluster-Site Approximation for the Entropy of Mixing in Multicomponent Solid Solutions, *Phys. Rev. B*, 1999, **59**, p 11221-11225
49. A.T. Dinsdale, SGTE Data for Pure Elements, *CALPHAD*, 1991, **15**, p 317-425
50. O. Redlich and A.T. Kister, Algebraic Representations of Thermodynamic Properties and the Classification of Solutions, *Ind. Eng. Chem.*, 1948, **40**, p 345-348
51. B. Sundman, S.G. Fries, and W.A. Oates, A Thermodynamic Assessment of the Au-Cu System, *CALPHAD*, 1998, **22**, p 335-354
52. T. Abe and B. Sundman, A Description of the Effect of Short Range Ordering in the Compound Energy Formalism, *CALPHAD*, 2003, **27**, p 403-408
53. T. Honda and Z. K. Liu, Unpublished, 2007
54. I. Ansara, T.G. Chart, A.F. Guillermet, F.H. Hayes, U.R. Kattner, D.G. Pettifor, N. Saunders, and K. Zeng, Thermodynamic Modelling of Solutions and Alloys—Schloss Ringberg, March 10 to March 16, 1996—Group 2: Alloy System I—Thermodynamic Modelling of Selected Topologically Close-Packed Intermetallic Compounds, *CALPHAD*, 1997, **21**, p 171-218
55. N. Dupin, I. Ansara, and B. Sundman, Thermodynamic Re-assessment of the Ternary System Al-Cr-Ni, *CALPHAD*, 2001, **25**, p 279-298
56. M. Hillert and M. Jarl, A Model for Alloying Effects in Ferromagnetic Metals, *CALPHAD*, 1978, **2**, p 227-238
57. W. Kohn and L. Sham, Self-Consistent Equations Including Exchange and Correlation Effects, *Phys. Rev.*, 1965, **140**, p 1133-1138
58. Y. Wang, Z.K. Liu, and L.Q. Chen, Thermodynamic Properties of Al, Ni, NiAl, and Ni_3Al from First-Principles Calculations, *Acta Mater.*, 2004, **52**, p 2665-2671
59. S.L. Shang, Y. Wang, D.E. Kim, and Z.K. Liu, First-Principles Thermodynamics from Phonon and Debye Model: Application to Ni and Ni_3Al, *Comput. Mater. Sci.*, Submitted, 2009
60. M. Born and R. Oppenheimer, Quantum Theory of Molecules, *Ann. Phys.-Berlin*, 1927, **84**, p 0457-0484
61. P. Hohenberg and W. Kohn, Inhomogeneous Electron Gas, *Phys. Rev. B*, 1964, **136**, p B864
62. D.M. Ceperley and B.J. Alder, Ground State of the Electron Gas by a Stochastic Method, *Phys. Rev. Lett.*, 1980, **45**, p 566-569
63. J.P. Perdew and A. Zunger, Self-Interaction Correction to Density-Functional Approximations for Many-Electron Systems, *Phys. Rev. B*, 1981, **23**, p 5048-5079
64. J.P. Perdew, K. Burke, and Y. Wang, Generalized Gradient Approximation for the Exchange-Correlation Hole of a Many-Electron System, *Phys. Rev. B*, 1996, **54**, p 16533-16539
65. J.P. Perdew, K. Burke, and Y. Wang, Generalized Gradient Approximation for the Exchange-Correlation Hole of a Many-Electron System (vol 54, pg 16 533, 1996), *Phys. Rev. B*, 1998, **57**, p 14999
66. J.P. Perdew and Y. Wang, Accurate and Simple Analytic Representation of the Electron-Gas Correlation-Energy, *Phys. Rev. B*, 1992, **45**, p 13244-13249
67. J.P. Perdew, K. Burke, and M. Ernzerhof, Generalized Gradient Approximation Made Simple, *Phys. Rev. Lett.*, 1996, **77**, p 3865-3868
68. G. Kresse and D. Joubert, From Ultrasoft Pseudopotentials to the Projector Augmented-Wave Method, *Phys. Rew. B*, 1999, **59**, p 1758-1775
69. A. Zunger, S.H. Wei, L.G. Ferreira, and J.E. Bernard, Special Quasirandom Structures, *Phys. Rev. Lett.*, 1990, **65**, p 353-356
70. S.H. Wei, L.G. Ferreira, J.E. Bernard, and A. Zunger, Electronic Properties of Random Alloys: Special Quasirandom Structures, *Phys. Rev. B*, 1990, **42**, p 9622-9649
71. A. Filippetti and N.A. Spaldin, Self-Interaction-Corrected Pseudopotential Scheme for Magnetic and Strongly-Correlated Systems, *Phys. Rev. B*, 2003, **67**, p 125109
72. V.I. Anisimov, F. Aryasetiawan, and A.I. Lichtenstein, First-Principles Calculations of the Electronic Structure and Spectra of Strongly Correlated Systems: The LDA+U Method, *J. Phys.-Condes. Matter*, 1997, **9**, p 767-808
73. A. Georges, G. Kotliar, W. Krauth, and M.J. Rozenberg, Dynamical Mean-Field Theory of Strongly Correlated Fermion Systems and the Limit of Infinite Dimensions, *Rev. Mod. Phys.*, 1996, **68**, p 13-125
74. J. Hafner, Ab Initio Simulations of Materials Using VASP: Density-Functional Theory and Beyond, *J. Comput. Chem.*, 2008, **29**, p 2044-2078
75. A.J. Cohen, P. Mori-Sanchez, and W.T. Yang, Insights into Current Limitations of Density Functional Theory, *Science*, 2008, **321**, p 792-794
76. J.M. Sanchez, Cluster Expansion and the Configurational Energy of Alloys, *Phys. Rew. B*, 1993, **48**, p R14013-R14015
77. A. van de Walle and M. Asta, Self-Driven Lattice-Model Monte Carlo Simulations of Alloy Thermodynamic Properties and Phase Diagrams, *Model. Simulat. Mater. Sci. Eng.*, 2002, **10**, p 521-538
78. V. Ozolins, C. Wolverton, and A. Zunger, Cu-Au, Ag-Au, Cu-Ag, and Ni-Au Intermetallics: First-Principles Study of Temperature-Composition Phase Diagrams and Structures, *Phys. Rev. B*, 1998, **57**, p 6427-6443
79. V.L. Moruzzi, J.F. Janak, and K. Schwarz, Calculated Thermal-Properties of Metals, *Phys. Rev. B*, 1988, **37**, p 790-799
80. A. van de Walle and G. Ceder, The Effect of Lattice Vibrations on Substitutional Alloy Thermodynamics, *Rev. Mod. Phys.*, 2002, **74**, p 11-45
81. X. Gonze, First-Principles Responses of Solids to Atomic Displacements and Homogeneous Electric Fields: Implementation

of a Conjugate-Gradient Algorithm, *Phys. Rev. B*, 1997, **55**, p 10337-10354
82. Y. Wang, D.Q. Chen, and X.W. Zhang, Calculated Equation of State of Al, Cu, Ta, Mo, and W to 1000 GPa, *Phys. Rev. Lett*, 2000, **84**, p 3220-3223
83. F. Kormann, A. Dick, B. Grabowski, B. Hallstedt, T. Hickel, and J. Neugebauer, Free Energy of bcc Iron: Integrated Ab Initio Derivation of Vibrational, Electronic, and Magnetic Contributions, *Phys. Rev. B*, 2008, **78**, p 033102
84. Y. Wang, L.G. Hector, H. Zhang, S.L. Shang, L.Q. Chen, and Z.K. Liu, Thermodynamics of the Ce Gamma-Alpha Transition: Density-Functional Study, *Phys. Rev. B*, 2008, **78**, p 104113
85. Y. Wang, L.G. Hector, Jr., H. Zhang, S.L. Shang, L.Q. Chen, and Z.K. Liu, Thermodynamic Framework for a System with Itinerant-Electron Magnetism, *J. Phys.: Condens. Matter*, 2009, **21**, p 326003
86. J. Iniguez and D. Vanderbilt, First-Principles Study of the Temperature-Pressure Phase Diagram of $BaTiO_3$, *Phys. Rev. Lett.*, 2002, **89**, p 115503
87. W. Zhong, D. Vanderbilt, and K.M. Rabe, First-Principles Theory of Ferroelectric Phase-Transitions for Perovskites—The Case of $BaTiO_3$, *Phys. Rev. B*, 1995, **52**, p 6301-6312
88. R. Car and M. Parrinello, Unified Approach for Molecular-Dynamics and Density-Functional Theory, *Phys. Rev. Lett.*, 1985, **55**, p 2471-2474
89. G. Kresse and J. Hafner, Ab Initio Molecular-Dynamics Simulation of the Liquid-Metal Amorphous-Semiconductor Transition in Germanium, *Phys. Rev. B*, 1994, **49**, p 14251-14269
90. S. Nose, A Unified Formulation of the Constant Temperature Molecular-Dynamics Methods, *J. Chem. Phys.*, 1984, **81**, p 511-519
91. S. Nose, A Molecular-Dynamics Method for Simulations in the Canonical Ensemble, *Mol. Phys.*, 1984, **52**, p 255-268
92. R. Iftimie, P. Minary, and M.E. Tuckerman, Ab initio molecular dynamics: Concepts, recent developments, and future trends, *Proc. Natl. Acad. Sci. USA*, 2005, **102**, p 6654-6659
93. R. Gao, X. Hui, H.Z. Fang, X.J. Liu, G.L. Chen, and Z.K. Liu, Structural Characterization of $Mg_{65}Cu_{25}Y_{10}$ Metallic Glass from Ab Initio Molecular Dynamics, *Comput. Mater. Sci.*, 2008, **44**, p 802-806
94. X. Hui, H.Z. Fang, G.L. Chen, S.L. Shang, Y. Wang, J.Y. Qin, and Z.K. Liu, Atomic Structure of $Zr_{41.2}Ti_{13.8}Cu_{12.5}Ni_{10}Be_{22.5}$ Bulk Metallic Glass Alloy, *Acta Mater.*, 2009, **57**, p 376-391
95. A.B. Belonoshko, L. Burakovsky, S.P. Chen, B. Johansson, A.S. Mikhaylushkin, D.L. Preston, S.I. Simak, and D.C. Swift, Molybdenum at High Pressure and Temperature: Melting from Another Solid Phase, *Phys. Rev. Lett.*, 2008, **100**, p 135701
96. Y. Wang, Z.K. Liu, L.Q. Chen, and C. Wolverton, First-Principles Calculations of Beta—Mg_5Si_6/Alpha-Al Interfaces, *Acta Mater.*, 2007, **55**, p 5934-5947
97. S.L. Shang, Y. Wang, and Z.K. Liu, First-Principles Elastic Constants of Alpha- and Theta-Al_2O_3, *Appl. Phys. Lett.*, 2007, **90**, p 101909
98. S. Ganeshan, S.L. Shang, H. Zhang, Y. Wang, M. Mantina, and Z.K. Liu, Elastic Constants of Binary Mg Compounds from First-Principles Calculations, *Intermetallics*, 2009, **17**, p 313-318
99. M. Mantina, Y. Wang, R. Arroyave, L.Q. Chen, Z.K. Liu, and C. Wolverton, First-Principles Calculation of Self-Diffusion Coefficients, *Phys. Rev. Lett.*, 2008, **100**, p 215901
100. Y. Zhong, C. Wolverton, Y.A. Chang, and Z.K. Liu, A Combined CALPHAD/First-Principles Remodeling of the Thermodynamics of Al-Sr: Unsuspected Ground State Energies by "Rounding up the (Un)usual Suspects, *Acta Mater.*, 2004, **52**, p 2739-2754
101. K. Ozturk, Y. Zhong, L.Q. Chen, C. Wolverton, J.O. Sofo, and Z.K. Liu, Linking First-Principles Energetics to CALPHAD: An Application to Thermodynamic Modeling of the Al-Ca Binary System, *Metall. Mater. Trans. A*, 2005, **36A**, p 5-13
102. S.H. Zhou, Y. Wang, C. Jiang, J.Z. Zhu, L.Q. Chen, and Z.K. Liu, First-Principles Calculations and Thermodynamic Modeling of the Ni-Mo System, *Mater. Sci. Eng. A*, 2005, **397**, p 288-296
103. Y. Zhong, M. Yang, and Z.K. Liu, Contribution of First-Principles Energetics to Al-Mg Thermodynamic Modeling, *CALPHAD*, 2005, **29**, p 303-311
104. W. Golumbfskie and Z.K. Liu, CALPHAD/First-Principles Re-modeling of the Co-Y Binary System, *J. Alloy. Compd.*, 2006, **407**, p 193-200
105. R. Arroyave and Z.K. Liu, Thermodynamic Modelling of the Zn-Zr System, *CALPHAD*, 2006, **30**, p 1-13
106. Y. Zhong, J. Liu, R.A. Witt, Y.H. Sohn, and Z.K. Liu, Al-2(Mg, Ca) Phases in Mg-Al-Ca Ternary System: First-Principles Prediction and Experimental Identification, *Scr. Mater.*, 2006, **55**, p 573-576
107. Y. Zhong, K. Ozturk, J.O. Sofo, and Z.K. Liu, Contribution of First-Principles Energetics to the Ca-Mg Thermodynamic Modeling, *J. Alloy. Compd.*, 2006, **420**, p 98-106
108. Y. Zhong, J.O. Sofo, A.A. Luo, and Z.K. Liu, Thermodynamics Modeling of the Mg-Sr and Ca-Mg-Sr Systems, *J. Alloy. Compd.*, 2006, **421**, p 172-178
109. D. Shin, R. Arroyave, and Z.K. Liu, Thermodynamic Modeling of the Hf-Si-O System, *CALPHAD*, 2006, **30**, p 375-386
110. J.E. Saal, D. Shin, A.J. Stevenson, G.L. Messing, and Z.K. Liu, First-Principles Calculations and Thermodynamic Modeling of the Al_2O_3-Nd_2O_3 System, *J. Am. Ceram. Soc.*, 2008, **91**, p 3355-3361
111. D. Shin, J.E. Saal, and Z.K. Liu, Thermodynamic Modeling of the Cu-Si System, *CALPHAD*, 2008, **32**, p 520-526
112. J.E. Saal, S. Shang, and Z.K. Liu, The Structural Evolution of Boron Carbide via Ab Initio Calculations, *Appl. Phys. Lett.*, 2007, **91**, p 231915
113. R. Arroyave, D. Shin, and Z.K. Liu, Ab Initio Thermodynamic Properties of Stoichiometric Phases in the Ni-Al System, *Acta Mater.*, 2005, **53**, p 1809-1819
114. R. Arroyave, A. van de Walle, and Z.-K. Liu, First-Principles Calculations of the Zn-Zr System, *Acta Mater.*, 2006, **54**, p 473-482
115. S.L. Shang, Y. Wang, H. Zhang, and Z.K. Liu, Lattice Dynamics and Anomalous Bonding in Rhombohedral As: First-Principles Supercell Method, *Phys. Rev. B*, 2007, **76**, p 052301
116. S.L. Shang, Y. Wang, R. Arroyave, and Z.K. Liu, Phase Stability in Alpha- and Beta-Rhombohedral Boron, *Phys. Rev. B*, 2007, **75**, p 092101
117. S.L. Shang, Y. Wang, and Z.K. Liu, First-Principles Calculations of Phonon and Thermodynamic Properties in the Boron-Alkaline Earth Metal Binary Systems: B-Ca, B-Sr, and B-Ba, *Phys. Rev. B*, 2007, **75**, p 024302
118. W.J. Golumbfskie, R. Arroyave, D. Shin, and Z.K. Liu, Finite-Temperature Thermodynamic and Vibrational Properties of Al-Ni-Y Compounds Via First-Principles Calculations, *Acta Mater.*, 2006, **54**, p 2291-2304

119. R. Arroyave and Z.K. Liu, Intermetallics in the Mg-Ca-Sn Ternary System: Structural, Vibrational, and Thermodynamic Properties from First Principles, *Phys. Rev. B*, 2006, **74**, p 174118
120. A. Ohno, A. Kozlov, R. Arroyave, Z.K. Liu, and R. Schmid-Fetzer, Thermodynamic Modeling of the Ca-Sn System Based on Finite Temperature Quantities from First-Principles and Experiment, *Acta Mater.*, 2006, **54**, p 4939-4951
121. A. Kozov, M. Ohno, R. Arroyave, Z.K. Liu, and R. Schmid-Fetzer, Phase Equilibria, Thermodynamics and Solidification Microstructures of Mg-Sn-Ca Alloys, Part 1: Experimental Investigation and Thermodynamic Modeling of the Ternary Mg-Sn-Ca System, *Intermetallics*, 2008, **16**, p 299-315
122. W.J. Golumbfskie, S.N. Prins, T.J. Eden, and Z.K. Liu, Predictions of the Al-rich region of the Al-Co-Ni-Y System Based Upon First-Principles and Experimental Data, *CALPHAD*, 2009, **33**, p 124-135
123. M. Hillert, A Solid-Solution Model for Inhomogeneous Systems, *Acta Metall.*, 1961, **9**, p 525-553
124. J.W. Cahn, Spinodal Decomposition in Cubic Crystals, *Acta Metall.*, 1962, **10**, p 179
125. T. Nishizawa, The 37th Honda Memorial Lecture—Progress of Calphad, *Mater. Trans. JIM*, 1992, **33**, p 713-722
126. T. Nishizawa, Effect of Magnetic Transition on Phase Equilibria in Iron Alloys, *J. Phase Equilib.*, 1995, **16**, p 379-389
127. C. Jiang, C. Wolverton, J. Sofo, L.Q. Chen, and Z.K. Liu, First-Principles Study of Binary bcc Alloys Using Special Quasirandom Structures, *Phys. Rev. B*, 2004, **69**, p 214202
128. D. Shin, R. Arroyave, Z.K. Liu, and A. Van de Walle, Thermodynamic Properties of Binary hcp Solution Phases from Special Quasirandom Structures, *Phys. Rev. B*, 2006, **74**, p 024204
129. D. Shin, A. van de Walle, Y. Wang, and Z.K. Liu, First-Principles Study of Ternary fcc Solution Phases from Special Quasirandom Structures, *Phys. Rev. B*, 2007, **76**, p 144204
130. D. Shin, Z.K. Liu, and C. Wolverton, Unpublished, 2009
131. C. Jiang, L.Q. Chen, and Z.K. Liu, First-Principles Study of Constitutional Point Defects in B2NiAl Using Special Quasirandom Structures, *Acta Mater.*, 2005, **53**, p 2643-2652
132. T. Wang, "An Integrated Approach for Microstructure Simulation: Application to Ni-Al-Mo Alloys," PhD Thesis, The Pennsylvania State University, 2006
133. S.J. Zhang, C. Brubaker, C. Jiang, M. Yang, Y. Zhong, Q.Y. Han, and Z.K. Liu, A Combined First-Principles Calculation and Thermodynamic Modeling of the F-K-Na System, *Mater. Sci. Eng. A*, 2006, **418**, p 161-171
134. A. van de Walle, M. Asta, and G. Ceder, The Alloy Theoretic Automated Toolkit: A User Guide, *CALPHAD*, 2002, **26**, p 539-553
135. D.W. Shin and Z.K. Liu, Enthalpy of Mixing for Ternary fcc Solid Solutions from Special Quasirandorn Structures, *CALPHAD*, 2008, **32**, p 74-81
136. I. Ansara, A.T. Dinsdale, and M.H. Rand, Ed., *COST 507: Thermochemical Database for Light Metal Alloys*, Vol 2, European Commission, 1998
137. R. Arroyave, D. Shin, and Z.K. Liu, Modification of the Thermodynamic Model for the Mg-Zr System, *CALPHAD*, 2005, **29**, p 230-238
138. S.L. Shang, Z.J. Liu, and Z.K. Liu, Thermodynamic Modeling of the Ba-Ni-Ti System, *J. Alloy. Compd.*, 2007, **430**, p 188-193
139. H. Zhang, Y. Wang, S.L. Shang, L.Q. Chen, and Z.K. Liu, Thermodynamic Modeling of Mg-Ca-Ce System by Combining First-Principles and CALPHAD Method, *J. Alloy. Compd.*, 2008, **463**, p 294-301
140. M. Mantina, "A First-Principles Methodology for Diffusion Coefficients in Metals and Dilute Alloys," Thesis, The Pennsylvania State University, 2008
141. C. Jiang, L.Q. Chen, and Z.K. Liu, First-Principles Study of Constitutional and Thermal Point Defects in B2PdIn, *Intermetallics*, 2006, **14**, p 248-254
142. P.A. Korzhavyi, A.V. Ruban, A.Y. Lozovoi, Y.K. Vekilov, I.A. Abrikosov, and B. Johansson, Constitutional and Thermal Point Defects in B2 NiAl, *Phys. Rev. B*, 2000, **61**, p 6003-6018
143. S. Prins, R. Arroyave, and Z.K. Liu, Defect Structures and Ternary Lattice Site Preference of the B2 Phase in the Al-Ni-Ru System, *Acta Mater.*, 2007, **55**, p 4781-4787
144. H.Z. Fang, X. Hui, G.L. Chen, and Z.K. Liu, Structural Evolution of Cu During Rapid Quenching by Ab Initio Molecular Dynamics, *Phys. Lett. A*, 2008, **372**, p 5831-5837
145. H.Z. Fang, X. Hui, G.L. Chen, R. Ottking, Y.H. Liu, J.A. Schaefer, and Z.K. Liu, Ab Initio Molecular Dynamics Simulation for Structural Transition of Zr During Rapid Quenching Processes, *Comput. Mater. Sci.*, 2008, **43**, p 1123-1129
146. T. Lida and R.I.L. Guthrie, *The Physical Properties of Liquid Metals*, Clarendon, Oxford, 1988
147. H.Z. Fang, X. Hui, G.L. Chen, and Z.K. Liu, Al-Centered Icosahedral Ordering in Cu46Zr46Al8 Bulk Metallic Glass, *Appl. Phys. Lett.*, 2009, **94**, p 091904
148. X. Hui, R. Gao, G.L. Chen, S.L. Shang, Y. Wang, and Z.K. Liu, Short-to-Medium-Range Order in $Mg_{65}Cu_{25}Y_{10}$ Metallic Glass, *Phys. Lett. A*, 2008, **372**, p 3078-3084
149. X. Hui, H.Z. Fang, G.L. Chen, S.L. Shang, Y. Wang, and Z.K. Liu, Icosahedral Ordering in $Zr_{41}Ti_{14}Cu_{12.5}Ni_{10}Be_{22.5}$ Bulk Metallic Glass, *Appl. Phys. Lett.,* 2008, **92**, p 201913
150. X. Hui, X.J. Liu, R. Gao, H.Y. Hou, H.Z. Fang, Z.K. Liu, and G.L. Chen, Atomic Structures of Zr-Based Metallic Glasses, *Sci. China Ser. G-Phys. Mech. Astron.*, 2008, **51**, p 400-413
151. Y. Wang and Z. K. Liu, Unpublished, 2009
152. Z.K. Liu, Thermodynamic Calculations and Phase Diagrams for Magnesium and its Alloys: Part II, *JOM*, 2009, **61**(5), p 67